1-1-2017

The Structure-Property Relations of Fetal Porcine Brain under Compressive and Tensile Loading

Courtney Jo White

The structure-property relations of fetal porcine brain under compressive and tensile loading

By

Courtney Jo White

A Thesis
Submitted to the Faculty of
Mississippi State University
in Partial Fulfillment of the Requirements
for the Degree of Master of Science
in Biomedical Engineering
in the Department of Agricultural and Biological Engineering

Mississippi State, Mississippi

May 2018

The structure-property relations of fetal porcine brain under compressive and tensile loading

By

Courtney Jo White

Approved:

_____

Lakiesha N. Williams
(Major Professor)

_____

Rajkumar Prabhu
(Committee Member)

_____

Jun Liao
(Committee Member)

_____

Michael D. Jones
(Committee Member)

_____

Michaela J. Beasley
(Committee Member)

_____

Steven H. Elder
(Graduate Coordinator)

_____

Jason M. Keith
Dean
Bagley College of Engineering

Name: Courtney Jo White

Date of Degree: May 4, 2018

Institution: Mississippi State University

Major Field: Biomedical Engineering

Major Professor: Lakiesha N. Williams

Title of Study: The structure-property relations of fetal porcine brain under compressive and tensile loading

Pages in Study 75

Candidate for Degree of Master of Science

Traumatic brain injury (TBI) in infants is detrimental to their development and can result in death; despite these risks, limited research has been conducted for this population. This studies purpose was to quantify biomechanical properties and microstructural changes after compressive and tensile loading of infant human brain surrogate, fetal porcine brain. Samples were loaded independently at strain rates of $0.00625s^{-1}$, $0.025s^{-1}$, and $0.10s^{-1}$ at strain levels of 0%, 15%, 30%, and 45% using the Mach-1^{TM} Micromechanical Testing Device. After loading to the specified strain level, samples were chemically fixed using 10% formalin. Samples were then stained using H&E to evaluate the microstructure. Results showed strain rate dependency and non-linearity with higher stress levels in compression than in tension. The histological analysis confirmed microstructural changes with statistically relevant deformations after loading. These results can assist in understanding infant TBI and help develop accurate head computational models and optimal protective headgear.

DEDICATION

I would not have completed this document without the love and support of my family and friends. My parents and brother have always been my biggest cheerleaders and continue to help me keep moving forward. I have also utilized the guidance and knowledge from my mentors during my time at Mississippi State University. All of the staff and students at MSU, most notably in the Agricultural and Biological Engineering Department, have assisted greatly in making my time here memorable and successful.

ACKNOWLEDGEMENTS

First, I would like to thank the Department of Agricultural and Biological Engineering (ABE) at Mississippi State University for supporting this project. Second, I would like to extend my gratitude to my graduate advisor Dr. Lakiesha Williams, as well as Dr. Raj Prabhu for their continued support and guidance in conducting this research. Further appreciation goes to the other members of my thesis committee Dr. Jun Liao, Dr. Michael D. Jones, and Dr. Michaela J. Beasley for their support and guidance. A word of thanks must also be given to the farm and office staff of Prestage Farms in Crawford Mississippi for assisting me in acquiring the stillborn fetal piglets used for testing in this study. The previous ABE research group who created the tension attachment used for mechanical testing should be recognized for their contribution and Dr. Michael Murphy for writing the Matlab GUI used for mechanical data analysis. Finally, I would like to thank Dr. Alicia Olivier from the College of Veterinary Medicine at Mississippi State University for her aid in the histological image analysis of my samples using ImageJ.

TABLE OF CONTENTS

DEDICATION ii

ACKNOWLEDGEMENTS iii

LIST OF TABLES vi

LIST OF FIGURES vii

CHAPTER

I. INTRODUCTION 1

1.1 References 5

II. LITERATURE REVIEW 8

2.1 Animal Models 8
2.2 Computer Models 10
2.3 Cadavers and Dummy Models 12
2.4 Human Studies 13
2.5 References 17

III. METHODS 19

3.1 Sample Preparation 19
3.2 Mach-1^{TM} Micromechanical Testing System 20
3.3 Compression Protocol 21
3.4 Tension Protocol 22
3.5 Histological Preparation after Compression 24
3.6 Histological Preparation after Tension 25
3.7 Image Analysis 28

IV. RESULTS 33

4.1 Mechanical Testing 33
4.1.1 Compression 33
4.1.2 Tension 34
4.2 Histology 36
4.2.2 Longitudinal Cross-section in Compression 37

4.2.3 Transverse Cross-section in Compression 40
4.2.4 Longitudinal Cross-section in Tension 42
4.2.5 Transverse Cross-section in Tension 45
4.2.6 Total Area of Cells 46
4.2.7 Cell Deformation 49

V. DISCUSSION 51

5.1 Validation of Using Porcine Specimens 51
5.2 Interpretation of Data 51
5.2.1 Analysis of Mechanical Testing in Compression 51
5.2.2 Analysis of Mechanical Testing in Tension 52
5.2.3 Histological Analysis of Longitudinal Cross-Section Under Compression 53
5.2.4 Histological Analysis of Transverse Cross-Section Under Compression 55
5.2.5 Histological Analysis of Longitudinal Cross-Section Under Tension 57
5.2.6 Histological Analysis of Transverse Cross-Section Under Tension 60
5.2.7 Total Area of Cells in the Tissue 62
5.2.8 Cell Deformation 63
5.3 Comparison of Existing Research 64
5.4 Clinical Implications 67
5.5 References 70

VI. CONCLUSION 72

6.1 Limitations and Future Works 73
6.2 References 75

LIST OF TABLES

4.1 Total cell area (μm^2) of cross-sections at strain rate 0.1 s^{-1} from control to 45% strain. (n=3 for each condition) 48

LIST OF FIGURES

3.1 Fresh fetal porcine brain tissue sample 20

3.2 Mach-1^{TM} Micromechanical Testing System compression testing apparatus 22

3.3 Mach-1^{TM} Micromechanical Testing System tension set up with in-house customized tension attachment 24

3.4 Schematic of cross-section planes of tissue samples for histological analysis 25

3.5 In-house customized tension attachment 27

3.6 Change in sample shape after mechanical testing 28

3.7 Schematic of area used on cross-sections for image analysis 30

3.8 (Left) MosaicJ image of compression sample strain rate 0.00625 s^{-1} at 45% strain. (Right) ImageJ cropped MosaicJ image for analysis. 30

3.9 Representative black and white threshold image for a compressed sample at a strain rate of 0.00625 s^{-1} at 45% strain. 31

4.1 Engineering stress-strain behavior of infant porcine brain under compression. 34

4.2 Engineering stress-strain behavior of fetal porcine brain under tensile loading. 35

4.3 Haematoxylin & Eosin stained slides of longitudinal cross-section after compression testing. 37

4.4 Mean (a) Area fraction and (b) Nearest neighbor distance of compressed tissue analyzed by longitudinal cross-section. 39

4.5 Mean (a) Area fraction and (b) Nearest neighbor distance of compressed tissue analyzed by tangential cross-section. 41

4.6 Mean (a) Area fraction and (b) Nearest neighbor distance of tensile tested tissue analyzed by longitudinal cross-section. 44

4.7 Mean (a) Area fraction and (b) Nearest neighbor distance of tensile tested tissue analyzed by tangential cross-section. 46

4.8 Total area of cells in tissue at 0.1 s^{-1} strain rate to 45% strain longitudinal and transverse cross-sections under compressive and tensile loading. Linear trend lines. (n=3 for each test)..... 48

4.9 Cell shape deformation at 0.1 s^{-1} strain rate to 45% strain longitudinal and transverse cross-sections under compressive and tensile loading. Linear trend lines. (n=3 for each test) 50

5.1 Schematic of tissue and cell deformation under compressive loading within the longitudinal cross-section. Solid arrows indicate loading direction and dashed arrows indicate tissue/cell movement direction. 54

5.2 Schematic of tissue and cell deformation under compressive loading within the transverse cross-section. Solid arrows indicate loading direction and dashed arrows indicate tissue/cell movement direction. 56

5.3 Schematic of tissue and cell deformation under tensile loading within the longitudinal cross-section. Solid arrows indicate loading direction and dashed arrows indicate tissue/cell movement direction. 58

5.4 Schematic of tissue and cell deformation under tensile loading within the transverse cross-section. Solid arrows indicate loading direction and dashed arrows indicate tissue/cell movement direction. 61

5.5 Comparison of stress-strain properties of porcine brain tissue compressed at strain rates of 0.1 s^{-1}, 0.025 s^{-1}, and 0.00625 s^{-1}. 66

CHAPTER I

INTRODUCTION

Traumatic brain injury (TBI) is a prevalent global problem that affects people of all ages.[19] Worldwide, there have been approximately 57 million people diagnosed annually with one or more TBIs and of these, 10 million resulted in hospitalization or death.[15,20] In the United States an average of 1.7 million TBIs occur each year, with 52,000 of these incidents resulting in death.[11,18,19] The average number of TBIs in children ages 0 to 14 is 511,000, and in adults 65 and older more than 237,000 TBIs occurred.[18,19]

For adults, the leading causes of TBI are falls, automotive accidents, and assaults.[19,22] Three of the main industries with a vested interest in studying TBI in adults and possible preventative measures are the automotive, sports, and military industries.[21] The automotive industries interest revolves around creating better crash test models to help prevent impact loading to the head during car crashes.[26] The sports industry is also concerned with studying impact loading to minimize TBI from player collisions and ground impact. [26] The military's focus is in understanding the effects of blasts from improvised explosive devices (IEDs) and the creation of better protective equipment.[29] Understanding TBI and the development of preventative measures for adults is important to the health and well-being of the population, as TBI can lead to immediate long term loss of motor or cognitive function through cell degeneration. The degeneration from

multiple occurrences of TBI in an individual or a severe singular TBI can lead to death.[2,14,23] These consequences of TBI in adults are the same as can be found in infants and children after sustaining a TBI.[1,8,9,16,27,31,32]

Over the past 20 years, research regarding infant TBI has increased.[1,4,8,10,12,16,17,25,27,28,32] However, for such severe consequences, TBI research in infants is understudied.[12,17] Falls are the leading cause of TBI sustained in infants and children.[3,10,13,24,25] To allow passage through the birth canal, the bones of the skull are connected by soft cartilage, which allows the bones to move and then regain their shape after birth. The bones of the skull grow together meeting at the skull's sutures post parturition and create the hardened skull of an adult.[16]

The infant brain, much like the skull, experiences a great amount of development after birth. During the time of development in children up to four years of age the central nervous system (CNS) undergoes accelerated growth and maturity.[5] There is an increase in the dendritic and axonal branching in the cerebrum accompanied by an increase in myelination of axons and a decrease in the water content.[7] Myelin is a white fatty substance made of the glial cell, oligodendrocytes, that surround the axons of the CNS to create an electrically insulating layer that enhances speed of signal conduction.[30] With this increase in myelination during brain maturation adult brains contain higher amounts of white matter than those found in infants. These differences in structure between the adult and infant brains lead to the belief that adult and infant brains would give different mechanical responses under load.[4,28,30]

Thibault et al. conducted a study comparing infant and adult porcine brain tissue, which found that under shear loads there was an increase in the shear modulus with age.

The testing was completed within three hours post-mortem on refrigerated fresh brain tissue to slow structural and physiological decomposition. A limitation to the study is the testing was conducted under the assumption that for mechanical characterization sample homogeneity is present. The shear testing was only conducted with samples from one location of the brain and one orientation.[28]

The presumption that differences in myelination allow for differences in mechanical response from tissues also lead to studies comparing the white and grey matter of the CNS. Weickenmeier et al. conducted a study determining how myelination affects the stiffness of brain tissue. Using pre-natal and post-natal brain samples, indentation testing was conducted within four hours post-mortem. This study found pre-natal brain tissue to be significantly softer than post-natal brain tissue. The tests also found white matter to be significantly stiffer than grey matter in both pre and post-natal brain.[30] These findings contradict those found by Budday et al., which concluded grey matter was stiffer than white matter. Budday et al. tested white and grey matter of adult human brain tissue, post autopsy, as isolated tissue samples under compression, tension, or shear forces.[4] These variations in findings illustrate the need for continued testing to understand how differences in structure during the stages of human brain development can affect how this tissue will be influenced by loading, the force seen when an infant is dropped or shaken.

In research conducted by Jones et al. on infant head impacts, a model of an infant head was created with a 3-D printed skull with sutures and filled with a balloon of gelatin to serve as the brain. The infant model was validated against known impact data and peak acceleration data on known infant post-mortem-human-surrogates. The skull was

modeled with noticeable sutures using polymers with different mechanical features for the sutures and skull, while the brain was modeled as one homogeneous substance, not allowing for different mechanical properties of the grey and white matter.[16] Cheng et al. conducted a study on infants to model shaken baby syndrome. The models contained correct anatomical features for the infant skull and contained a fluid boundary and membrane surrounding the brain but used adult mechanical data for the validation of the brain model.[6]

As shown, previous research has improved the body of literature on infant TBI but has not focused on the structure-property relationship or the correlation between structure and function of fetal tissue after quasi-static loading. In this study, quasi-static uniaxial compressive and tensile testing was conducted on fetal porcine brain tissue followed by histology to create a multifaceted analysis of the effects of loading on the structure-property relationship of fetal brain tissue. With this enhanced understanding of the mechanical behaviors of fetal porcine brain tissue and how loading affects the microstructure, more accurate virtual models can be created for testing. Thus, the motivation of this study; to correlate structure and function of fetal porcine brain tissue. Greater accuracy of infant testing models through the understanding of the mechanical properties and changing microstructure of the infant brain during the first few weeks after birth will allow for less live animal testing and creation of faster testing techniques and prediction models of TBI.

1.1 References

1. Anderson, V., C. Catroppa, S. Morse, F. Haritou, and J. Rosenfeld. Recovery of intellectual ability following traumatic brain injury in childhood: impact of injury severity and age at injury. *Pediatr. Neurosurg*. 32:282–90, 2000.

2. Brooks, N., W. McKinlay, C. Symington, A. Beattie, and L. Campsie. Return to work within the first seven years of severe head injury. *Brain Inj*. 1:5–19.

3. Bruce, D. A. Head injuries in the pediatric population. *Curr. Probl. Pediatr*. 20:61–107, 1990.

4. Budday, S., G. Sommer, C. Birkl, C. Langkammer, J. Haybaeck, J. Kohnert, M. Bauer, F. Paulsen, P. Steinmann, E. Kuhl, and G. A. Holzapfel. Mechanical characterization of human brain tissue. *Acta Biomater*. 48:319–340, 2017.

5. Calder, I. M., I. Hill, and C. L. Scholtz. Primary brain trauma in non-accidental injury. J. *Clin. Pathol*. 37:1095–1100, 1984.

6. Cheng, J., I. C. Howard, and M. Rennison. Study of an infant brain subjected to periodic motion via a custom experimental apparatus design and finite element modelling. *J. Biomech*. , 2010.doi:10.1016/j.jbiomech.2010.07.023

7. Dobbing, J. The later growth of the brain and its vulnerability. *Pediatrics* 53:2–6, 1974.

8. Ewing-Cobbs, L., M. E. Miner, J. M. Fletcher, and H. S. Levin. Intellectual, motor, and language sequelae following closed head injury in infants and preschoolers. *J. Pediatr. Psychol.* 14:531–47, 1989.

9. Ewing-Cobbs, L., M. R. Prasad, S. H. Landry, L. Kramer, and R. DeLeon. Executive Functions Following Traumatic Brain Injury in Young Children: A Preliminary Analysis. Dev. *Neuropsychol*. 26:487–512, 2004.

10. Falk, A.-C. Age differences in brain injury characteristics. Dev. *Neurorehabil*. 13:315–21, 2010.

11. Faul, M., L. Xu, M. M. Wald, V. Coronado, and A. M. Dellinger. Traumatic brain injury in the United States: national estimates of prevalence and incidence, 2002-2006. *Inj. Prev.* 16:A268–A268, 2010.

12. Gotschall, C. S., P. H. Papero, H. M. Snyder, D. L. Johnson, W. J. Sacco, and M. R. Eichelberger. Comparison of Three Measures of Injury Severity in Children with Traumatic Brain Injury. *J. Neurotrauma* 12:611–619, 1995.

13. Guerrero, J. L., D. J. Thurman, and J. E. Sniezek. Emergency department visits associated with traumatic brain injury: United States, 1995-1996. *Brain Inj.* 14:181–6, 2000.

14. Humphreys, I., R. L. Wood, C. J. Phillips, and S. Macey. The costs of traumatic brain injury: a literature review. *Clinicoecon. Outcomes Res*. 5:281–7, 2013.

15. Hyder, A. A., C. A. Wunderlich, P. Puvanachandra, G. Gururaj, and O. C. Kobusingye. The impact of traumatic brain injuries: a global perspective. *NeuroRehabilitation.* 22:341–53, 2007.

16. Jones, M., D. Darwall, G. Khalid, R. Prabhu, A. Kemp, O. J. Arthurs, and P. Theobald. Development and validation of a physical model to investigate the biomechanics of infant head impact. *Forensic Sci.* Int. 276:111–119, 2017.

17. Kraus, J. F. Epidemiological features of brain injury in children: Occurrence, children at risk, causes and manner of injury, severity, and outcomes. Traumatic head injury in children. 22–39, 1995.

18. Langlois, J. A., W. Rutland-Brown, and K. E. Thomas. Traumatic brain injury in the United States: Emergency department visits, hospitalizations, and deaths. Centers for Disease Control and Prevention, National Center for Injury Prevention and Control, 2004.

19. Langlois, J. A., W. Rutland-Brown, and K. E. Thomas. Traumatic brain injury in the United States: Emergency department visits, hospitalizations, and deaths. Centers for Disease Control and Prevention, National Center for Injury Prevention and Control, 2006.

20. Langlois, J. A., W. Rutland-Brown, and M. M. Wald. The epidemiology and impact of traumatic brain injury: a brief overview. *J. Head Trauma Rehabil*. 21:375–8.

21. Leo, P., and M. McCrea. Epidemiology. CRC Press/Taylor and Francis Group, 2016.at <http://www.ncbi.nlm.nih.gov/pubmed/26583186>

22. Maas, A. I., N. Stocchetti, and R. Bullock. Moderate and severe traumatic brain injury in adults. 2008.

23. Murray, C. J., and A. D. Lopez. Alternative projections of mortality and disability by cause 1990–2020: Global Burden of Disease Study. *Lancet* 349:1498–1504, 1997.

24. Pascucci, R. C. Head trauma in the child. Intensive Care Med. 14:185–195, 1988.

25. Ponce, E., and D. Ponce. Modeling Neck and Brain Injuries in Infants. IEEE *Comput. Graph. Appl.* 31:90–96, 2011.

26. Saraf, H., K. T. Ramesh, A. M. Lennon, A. C. Merkle, and J. C. Roberts. Mechanical properties of soft human tissues under dynamic loading. *J. Biomech*. 40:1960–1967, 2007.

27. Stancin, T., D. Drotar, H. G. Taylor, K. O. Yeates, S. L. Wade, and N. M. Minich. Health-related quality of life of children and adolescents after traumatic brain injury. *Pediatrics* 109:E34, 2002.

28. Thibault, K. L., and S. S. Margulies. Age-dependent material properties of the porcine cerebrum: effect on pediatric inertial head injury criteria. *J. Biomech*. 31:1119–1126, 1998.

29. Warden, D. Military TBI during the Iraq and Afghanistan wars. *J. Head Trauma Rehabil*. 21:398–402.

30. Weickenmeier, J., R. de Rooij, S. Budday, T. C. Ovaert, and E. Kuhl. The mechanical importance of myelination in the central nervous system. *J. Mech. Behav. Biomed. Mater*. 0–1, 2017.doi:10.1016/j.jmbbm.2017.04.017

31. Yeates K. O. Pediatric closed-head injury. In: Yeates KO, Ris MD, Taylor HG, editors. Pediatric neuropsychology: Research, theory, and practice. New York, NY: Guilford; 92–116, 2000.

32. Yeates, K. O., and H. G. Taylor. Predicting premorbid neuropsychological functioning following pediatric traumatic brain injury. *J. Clin. Exp. Neuropsychol*. 19:825–837, 1997.

CHAPTER II

LITERATURE REVIEW

2.1 Animal Models

Animal models are often used as surrogates for studying the physiological and mechanical systems of the human body.[1,2,3,6,10,12,15,17] Using these models can be very helpful, however, animals are usually good for modeling simple individual systems or body mechanisms.[1] An animal model is chosen based on the goal and objectives of the specific research, as well as the specific animals relationship to human physical systems and monetary costs.[1,11] There are many assumptions and some limitations when using animal surrogates for studying the human brain. The fit for an appropriate animal model is especially important because of how essential in vivo models are in understanding neurotrauma and our ability to develop better protective devices and neuroprotective therapies.[1]

Porcine models have been used extensively as surrogates for studying TBI.[2,3,12,13,15,18] Pigs are often used as models for human brain testing because their brain develops gyri and sulci like a humans. The porcine brain is also geometrically shaped closer to that of a human brain than the elongated brain of the rat.[1]

Shaken baby syndrome is an often deadly trauma inflicted on babies when they are violently shaken. The babies' head undergoes excessive movement due to their necks inability to support and limit movement of their head. Survivors of shaken baby

syndrome have a more than 50% chance of developing chronic neurological problems.[1,4,9] In the University of Pennsylvania study, three to five day old piglets were used to model shaken baby syndrome. The piglets were anesthetized and given either a single rapidly accelerating head rotation or a double rotation. Six hours after the head rotations the piglets were euthanized and the brains were evaluated for axonal injury. The piglets subjected to two rotations had a significant increase in damaged axons compared to piglets with only one rotation. Another significant difference between the two head rotational groups studied was that the piglets with double head rotations had a significant drop in blood pressure during the research compared to the piglets with one rotation. The drop in blood pressure indicates a global response through the piglets body due to the localized brain injury after rotation. The study found that damage to an immature brain can occur even under quasi-static loading during rotation with no impact involved.[1]

Coats et al. conducted a similar study using piglets to model shaken baby syndrome where the piglets were tested with low-velocity head rotations.[2] These piglets were sacrificed to determine how injury propagated after 6 hours, 24 hours, or 6 days. Similarly to the aforementioned study from the University of Pennsylvania, single and multiple head rotation damage was compared. However, in this study the hyper flexion and extension of the piglet's neck was prevented during rotation. The piglets with multiple head rotations had a higher amount of axonal injury than those with only a single head rotation. This corroborated the data from the previously reviewed piglet study that multiple head rotations resulted in higher axonal injury. Higher amounts of axonal injury was found in both groups the further from the time of testing.[2]

Another study by a team from the University of Adelaide on shaken baby syndrome was conducted using a lamb model.[6] They evaluated whether head impact and shaking caused severe brain injury and death. The researchers selected lambs because of their morphologically similar brains to humans and their weak neck muscles, like an infant. Four control lambs were anesthetized but not shaken. Nine lambs were anaesthetized and then manually shaken by hand with enough force to ensure hyper-flexion and extension of the neck. Six hours after being anesthetized and some being shaken, the lambs were euthanized. Damage to the axons was found in all of the shaken lambs, confirming the pig studies that shaking and rotation of the head can cause axonal injury. A meaningful follow-up study would be to repeat the lamb study without hyper-flexion/extension of the neck. An additional improvement would be to use a mechanical system for the head rotations instead of conducting them by hand. A significant difference in the magnitude of the damage was found to be dependent on weight of the animal. The lambs with a lower weight had a significantly larger amount of damaged axons in the white matter of their brain. Three of the lambs that were in the lower weight category of those tested also died unexpectedly after being shaken. This information helped the researchers to conclude that severe injury and death could possibly occur in an infant just from being shaken, especially if the infant is of a smaller weight and size.[6]

2.2 Computer Models

Computer models are being increasingly utilized to allow for decreased use of live animals in laboratory testing. These verified and validated computer models are created using live animal studies. In a study by Coats et al., a model was created of a 4-week-old piglet head and scaled to the size of a 3 to 5 day old piglet.[3] The model was created with

the brain either fixed or spring attached to the skull at 5 contact points to ensure a secure boundary. The computational results were compared to the strains found in brain as well as brain and skull displacement studies of 3 to 5 day old piglets. Once the results were a statistical match, the model was used for testing. The brain and brainstem were represented as a homogenous and viscoelastic material. However, the brain is not homogenous, with different cells contained within the white and grey matter portions. This assumption could be an influence that resulted in the model being less accurate. The stiffness and elastic modulus for the model were obtained from literature for fetal dura, while the skull was modeled as a hard, rigid body. The accuracy of the model was increased by adding the dura to the model and assigning it its own properties in relation to the brain and skull. Using the model that closely matched with the data from live animal studies, rapid head rotations were simulated. Both models (fixed and spring) of the brain and skull resulted in data that was comparable to those in the live animal studies, but the spring attached model gave the best indication of possible brain hemorrhaging.[3] This is as expected since the brain is attached to the skull via the dura, a connective tissue layer surrounding the cerebral spinal fluid. The connective attachment of the dura gives the anatomy a more spring-like than fixed atachment.

Animal models, both experimental and computational, are important for research and understanding the biology and mechanics needed for developing safety countermeasures. The end goal for these animal studies is ultimately to better understand TBI in humans. Therefore, human models are also an integral part of understanding how the human body would react or function in a situation. Inducing TBI in living humans however is highly unethical. Thus, much of the human research is completed through

hospital records and autopsy results or using an anthropometric dummy or computer program to simulate the human.[1,6,11,12]

2.3 Cadavers and Dummy Models

Duhaime et al. reviewed 48 cases of infants and young children between the ages of one month and two years old that had been diagnosed with shaken baby syndrome.[5] Of the 48 cases reviewed, there were thirteen fatalities. Autopsies performed for every case of fatality showed evidence of blunt force trauma. Blunt force trauma coupled with shaking caused an increase in intracranial pressure that led to the infant's death. In this study, the researchers also created models from "Just Born" dolls, representative of one-month-old human infants with different skull and neck parameters. The model infants were shaken and impacted against either a padded or unpadded surface. An accelerometer was placed onto the head of the model for measurements of the force on the head during shaking and impact. The padded surface was found to decrease the magnitude of acceleration on the models head; however, even on the padded surface the impact was found to be enough to enter into the injurious range. The researchers concluded that shaking alone is not sufficient to cause shaken baby syndrome, which contradicts the conclusion of the lamb study that shaking alone was enough to cause death. This may be because the dolls did not have a model in a low enough weight class to model the same degree of injury. It could also show that a different factor other than the acceleration caused death.

Another study used data from infant cadavers to evaluate the kinematics of the infant neck by evaluating their bending and tensile forces.[14] The forces found from the cadavers were then incorporated into models of an infant to determine the damage to the

infant's head and neck after a fall. These real human models are generally created using kinematic data from adults scaled down to the infants. Head-first falls onto the occipital and parietal portions of the head were evaluated against the original model using adult kinematics. It was found that the model using infant neck kinematics had a significantly smaller impact force as well as peak angular accelerations.[14] These differences show the importance of accurate models for infant biomechanics in determining the amount of possible injury an infant could sustain. Without an accurate assessment of the amount of injury sustained to an infant, proper steps cannot be taken to intervene and treat the damage. Without an accurate assessment it is also harder to give a correct evaluation of how children could have sustained their injuries when admitted into a hospital or in a court.

2.4 Human Studies

In a study from the University of Louisville, 79 cases of children admitted to the hospital with a history of low falls were evaluated for severity of injury.[16] It was found that the greater the height and velocity of the fall, the larger the impact on injury. It was also found that like in the head rotational study with the lambs, the smaller the child, the greater the injury sustained. This also is suggested in the study with infant doll models in that there might not have been a doll for a weight class small enough to show the difference in injury. Unlike in the lamb study, there were no instances of death even in the smaller children.[16] This also indicates as well there might be an underlying factor along with weight causing subject death. A possible factor for subject death could be poor health brought on by malnutrition. A smaller animal or child could be more

malnourished than their counterparts and their bodies' ability to heal and protect its cells, such as its neurons, could be affected creating a higher likelihood of death.

The inconsistency of the conclusions from these studies show that different models can give different results, especially between infant live animal models and surrogate models such as the dolls and simulations. Possible reasons for this include biological processes that are not addressed in models not containing a physiological brain with a cerebral spinal fluid component. Another factor influencing the validity of models in comparison to live infants is the use of adult mechanical data as criteria testing. More testing is needed of animal and surrogate models to understand the reason for these differences. A way to lessen the difference in the results from between models and expand our understanding for infant head models is the use of improved methods of data acquisition. We can do this by using methods found in adult testing and applying it to the acquisition of data in infant testing for infant models.

A Stanford University study was conducted using athletes wearing mouthguards that allowed results from 6 degrees of freedom instead of the usual 3.[8] The mouthguards measured 3 degrees of freedom in both the rotational and translational directions. The athletes were evaluated for a mild traumatic brain injury (mTBI) after a head impact and head movements were evaluated. The peak principle strain from the corpus callosum, a measurement of the 6 degrees of freedom model, was the most predictive of mTBI. In all, the six degrees of freedom model appeared to better predict mTBI than either of the three degrees of freedom model. Mouthpieces are not realistic methods to gain results in infants. However, the knowledge that the six degrees of freedom is a better way to collect results might help to shape how future studies should be handled. The knowledge of the

corpus callosum peak strain being a good predictor of mTBI could also be used in future testing.[8]

Infants are vulnerable to TBI due to both their inability to function on their own and the fact that their developing bodies are fragile. This is most notable with respect to weak neck muscles supporting an infant's soft skull and still extremely malleable brain. This can lead to long term damage of their brain and subsequent physical or mental functional disability up to death.[11] Strategies for better understanding when a TBI has occurred, as well as preventative measures and the rehabilitation of infants using therapies can be developed utilizing research to make the infants futures brighter.[7]

This current study of infant TBI gives age-specific mechanical data for the first month of a human infants' life using stillborn, full term fetal porcine brain tissue. The compression and tension mechanical impact data of fresh native tissue at this age negates the need for scaling down mechanical data from older age groups. Not scaling down from adult data allows for more accurate model development for infant heads and brains and for comparison of test results to confirm accuracy. The histological data gathered allows for determination of the impact on physiological properties of tissues after loading. A greater understanding of the change in microstructure after loading and how physiological properties might influence this change can help to determine the larger impact this change in microstructure can have on the infant. The mechanical and microstructural components can eventually be combined with the cells of the infant brain tissue incorporated within an FE model and then used to determine accuracy of the models mechanical data and microstructural change. The infant specific computer or

dummy model could then be used to understand and model TBIs without the use of *in vivo* animal models.

2.5 References

1. Cernak, I. Animal models of head trauma. *NeuroRX* 2:410–422, 2005.

2. Coats, B., G. Binenbaum, C. Smith, R. L. Peiffer, C. W. Christian, A.-C. Duhaime, and S. S. Margulies. Cyclic Head Rotations Produce Modest Brain Injury in Infant Piglets. *J. Neurotrauma* 34:235–247, 2017.

3. Coats, B., S. A. Eucker, S. Sullivan, and S. S. Margulies. Finite element model predictions of intracranial hemorrhage from non-impact, rapid head rotations in the piglet. *Int. J. Dev. Neurosci.* 30:191–200, 2012.

4. Duhaime, A.-C., C. W. Christian, L. B. Rorke, and R. A. Zimmerman. Nonaccidental Head Injury in Infants — The "Shaken-Baby Syndrome." *N. Engl. J. Med.* 338:1822–1829, 1998.

5. Duhaime, A.-C., T. A. Gennarelli, L. E. Thibault, D. A. Bruce, S. S. Margulies, and R. Wiser. The shaken baby syndrome. *J. Neurosurg.* 66:409–415, 1987.

6. Finnie, J. W., P. C. Blumbergs, J. Manavis, R. J. Turner, S. Helps, R. Vink, R. W. Byard, G. Chidlow, B. Sandoz, J. Dutschke, and R. W. G. Anderson. Neuropathological changes in a lamb model of non-accidental head injury (the shaken baby syndrome). *J. Clin. Neurosci.* 19:1159–1164, 2012.

7. Goldsmith, W., and J. Plunkett. A biomechanical analysis of the causes of traumatic brain injury in infants and children. *Am. J. Forensic Med. Pathol.* 25:89–100, 2004.

8. Hernandez, F., L. C. Wu, M. C. Yip, K. Laksari, A. R. Hoffman, J. R. Lopez, G. A. Grant, S. Kleiven, and D. B. Camarillo. Six Degree-of-Freedom Measurements of Human Mild Traumatic Brain Injury. *Ann. Biomed. Eng.* 43:1918–1934, 2015.

9. Marín-Padilla, M., J. Parisi, D. Armstrong, S. Sargent, and J. Kaplan. Shaken infant syndrome: developmental neuropathology, progressive cortical dysplasia, and epilepsy. *Acta Neuropathol.* 103:321–332, 2002.

10. McIntosh, T. K., R. Vink, L. Noble, I. Yamakami, S. Fernyak, H. Soares, and A. L. Faden. Traumatic brain injury in the rat: Characterization of a lateral fluid-percussion model. *Neuroscience* 28:233–244, 1989.

11. Meythaler, J. M., J. D. Peduzzi, E. Eleftheriou, and T. A. Novack. Current concepts: Diffuse axonal injury–associated traumatic brain injury. *Arch. Phys. Med. Rehabil.* 82:1461–1471, 2001.

12. Raghupathi, R., M. F. Mehr, M. A. Helfaer, and S. S. Margulies. Traumatic Axonal Injury is Exacerbated following Repetitive Closed Head Injury in the Neonatal Pig. *J. Neurotrauma* 21:307–316, 2004.

13. Sillesen, M., L. S. Rasmussen, G. Jin, C. H. Jepsen, A. Imam, J. O. Hwabejire, I. Halaweish, M. DeMoya, G. Velmahos, P. I. Johansson, and H. B. Alam. Assessment of coagulopathy, endothelial injury, and inflammation after traumatic brain injury and hemorrhage in a porcine model. *J. Trauma Acute Care Surg.* 76:12–20, 2014.

14. Sullivan, S., B. Coats, and S. S. Margulies. Biofidelic neck influences head kinematics of parietal and occipital impacts following short falls in infants. *Accid. Anal. Prev.* 82:143–153, 2015.

15. Thibault, K. L., and S. S. Margulies. Age-dependent material properties of the porcine cerebrum: effect on pediatric inertial head injury criteria. *J. Biomech.* 31:1119–1126, 1998.

16. Thompson, A. K., G. Bertocci, W. Rice, and M. C. Pierce. Pediatric short-distance household falls: Biomechanics and associated injury severity. *Accid. Anal. Prev.* 43:143–150, 2011.

17. Weickenmeier, J., R. de Rooij, S. Budday, T. C. Ovaert, and E. Kuhl. The mechanical importance of myelination in the central nervous system. *J. Mech. Behav. Biomed. Mater.* 0–1, 2017.doi:10.1016/j.jmbbm.2017.04.017

18. Zhu, F., P. Skelton, C. C. Chou, H. Mao, K. H. Yang, and A. I. King. Biomechanical responses of a pig head under blast loading: a computational simulation. *Int. j. numer. method. biomed. eng.* 29:392–407, 2013.

CHAPTER III

METHODS

3.1 Sample Preparation

Stillborn fetal piglets were acquired from a local abattoir (Prestage Farms, Crawford, MS) the morning of death. Brain samples were tested immediately following dissection. The piglets were stored in a cooler of ice to slow the rate of decomposition and transported to the dissection lab of the Agricultural and Biological Engineering building at Mississippi State University. In the lab, intact brains were surgically extracted from the fetal piglets and kept hydrated using a spray bottle of 0.01M phosphate buffered saline (PBS) (Sigma-Aldrich, St. Louis, MO) solution once every ten minutes to preserve the samples structural integrity. From the brain of each of the 90 piglets (weight ~ 680g), two cylindrical brain samples approximately 22 mm in diameter and 11 mm in height were dissected (Figure 3.1). A tissue sample was taken from each hemisphere of the extracted brains using a fabricated stainless-steel die (Agricultural and Biological Engineering, Mississippi State University) 22 mm in diameter (Figure 3.1). The longitudinal extraction through the frontal, and parietal lobes of the brain yielded samples characterized by sulci and gyri on the upper surface. The samples were extracted from one piglet at a time and immediately tested before the next sample extraction to best sustain the samples' microstructural integrity. All samples were tested within 30 minutes of extraction and all tests were completed within 3 hours from the time the piglets were obtained.

Figure 3.1 Fresh fetal porcine brain tissue sample

3.2 Mach-1™ Micromechanical Testing System

The Mach-1™ Micromechanical Testing System (BIOSYNTECH micromechanical systems, Canada) composed of the following: the Mach-1™ testing apparatus, 10 kg load cell, load cell amplifier, Universal Motion Controller/Driver-Model ESP300, and computer with Mach-1™ Motion software. Prior to testing, preliminary Mach-1™ program sequences were built. In the sequence-managing window, the Find Contact command was used to precisely measure the initial height of the test specimen. The height of the specimen was then used to calculate the amplitude (mm) and velocity

(mm/s) for each test and input into the Move Relative function. The load and position automatically zeroed out before the Move Relative function was begun and the compression or tension test was performed at one of three strain rates, 0.00625 s^{-1}, 0.025 s^{-1}, or 0.1 s^{-1} and either 15%, 30%, or 45% strain.

3.3 Compression Protocol

For compression testing, each sample was placed into a stainless steel cylindrical platform with raised sides and placed onto the Mach-1^{TM} as shown in Figure 3.2. A room temperature (22°C) PBS bath was created and the sample submerged in the PBS within the stainless-steel chamber to mimic the conditions of the brain in CSF. The Mach-1^{TM} was calibrated before each test and the programmed settings lowered the circular platen attached to the 10 kg load cell onto the sample until a 5.00 g load was read. Forty-five samples were compressed at one of three strain rates, 0.00625 s^{-1}, 0.025 s^{-1}, or 0.10 s^{-1} and compressed to 15%, 30%, or 45% strain level. The time (s), load (gf), and displacement (mm) from the tests was recorded by the Mach-1 motion software and used to generate stress-strain curves using an in-house Matlab (R2017a, The MathWorks, Inc., Natick, MA) GUI.

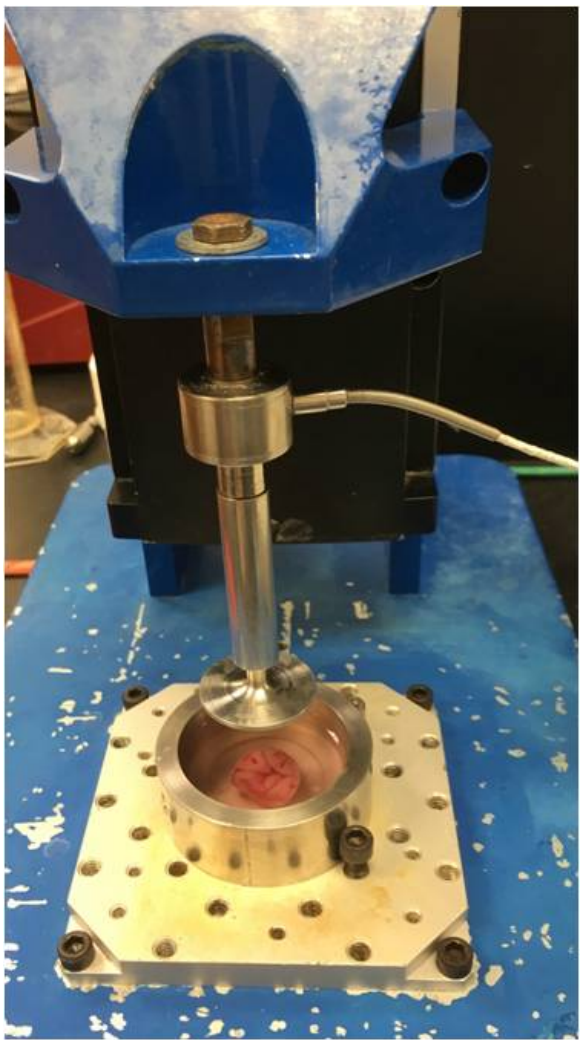

Figure 3.2 Mach-1^{TM} Micromechanical Testing System compression testing apparatus

3.4 Tension Protocol

The 10 kg load cell was also utilized for tensile testing using a custom attachment, as shown in Figure 3.3, and tested without a PBS bath to allow adhesion of the sample to the tension attachments using surgical glue. The Mach-1^{TM} was calibrated before securing the tension attachment before each test. After securing the sample to the bottom of the attachment with surgical glue, the top of the attachment was lowered until a 5.00 g

load was read to ensure the top of the attachment contacted the sample. A wait time of one minute was given to allow the surgical glue to dry before tension testing was begun. Forty-five samples were then pulled in tension at a strain rate of 0.00625 s^{-1}, 0.025 s^{-1}, or 0.10 s^{-1}. For each strain rate, the samples were pulled in tension to 15%, 30%, or 45% strain. The time (s), load (gf), and displacement (mm) from the tests were collected using the Mach-1^{TM} motion software and used to generate the stress-strain curves for analysis using the in-house Matlab GUI.

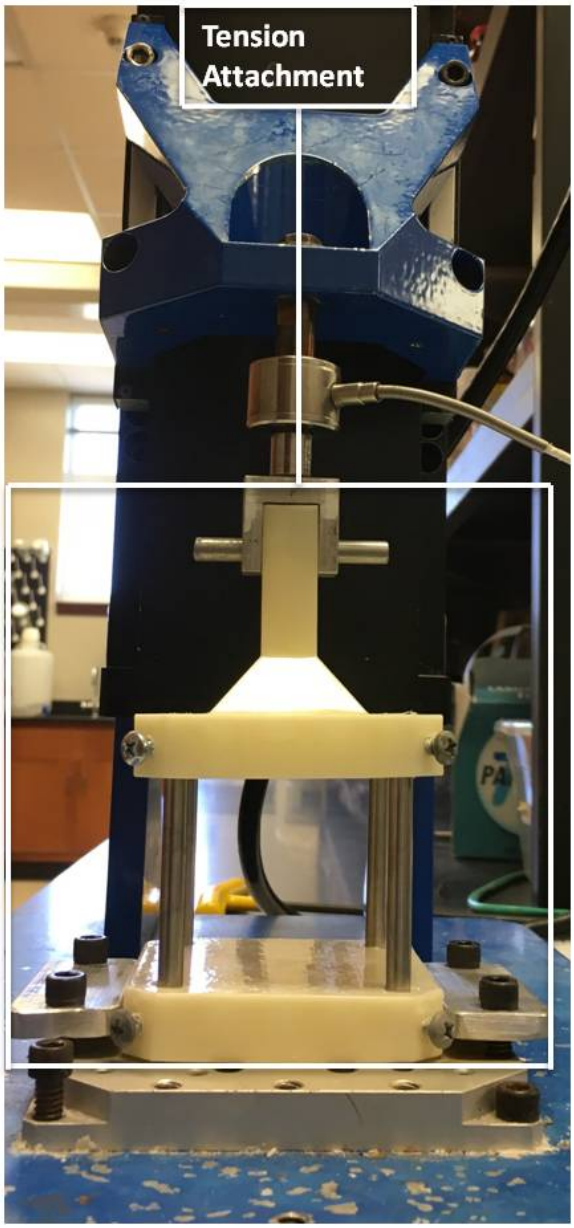

Figure 3.3 Mach-1^{TM} Micromechanical Testing System tension set up with in-house customized tension attachment

3.5 Histological Preparation after Compression

The test was automatically stopped by the Mach-1^{TM} following compression to the specified strain level tested of 15%, 30%, or 45%. Remaining in the compressed

state, the PBS solution was pipette out of the raised compression platform. The PBS bath was replaced by 10% Formalin (Sigma-Aldrich, St. Louis, MO) to chemically fix the sample. The samples were then fixed in 10% Formalin for 24 hours before being removed from their compressed state on the Mach-1^{TM}. After 24 hours of fixation, sample relaxation was believed to be minimal. Following removal, samples were fixed in 10% Formalin for an additional week in a labeled, sterilized, and sealed container. The fixed samples were then surgically cut into longitudinal and transverse cross-sections (Figure 3.4) and sent to the Mississippi State University College of Veterinary Medicine Diagnostic Laboratory for Haematoxylin & Eosin (H&E) staining.

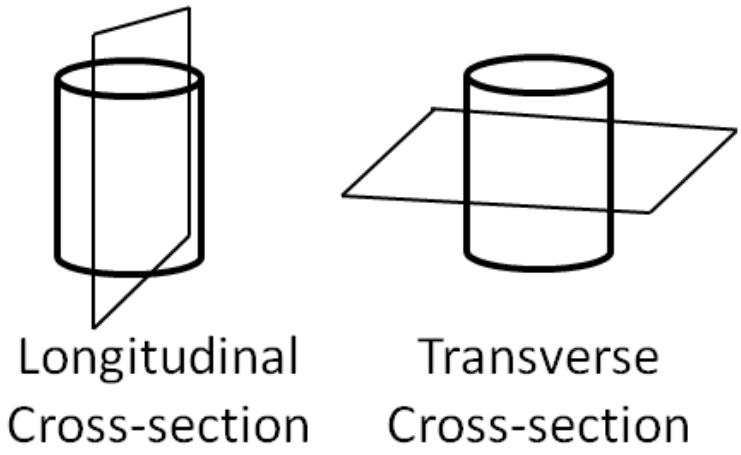

Figure 3.4 Schematic of cross-section planes of tissue samples for histological analysis

3.6 Histological Preparation after Tension

A specialized attachment (Figure 3.5) was created by our team for a previous study. We adapted the fixture for this portion of the study so the attachment secures to the Mach-1^{TM} and can be removed after testing without displacing the sample. After the

sample was pulled in tension the top four screws attached to the platform were tightened to prevent the samples from changing length. The attachment with the sample inside was then removed from the Mach-1™ and put into a container to create a sealed 10% Formalin bath to chemically fix the sample for 24 hours. After 24 hours, the samples were surgically removed from the attachment and fixed in fresh 10% formalin within a labeled, sterilized, and sealed container. After a week of additional fixation, the fixed samples were then cut into longitudinal and transverse cross-sections and given to the Mississippi State University College of Veterinary Medicine Diagnostic Laboratory for H & E staining.

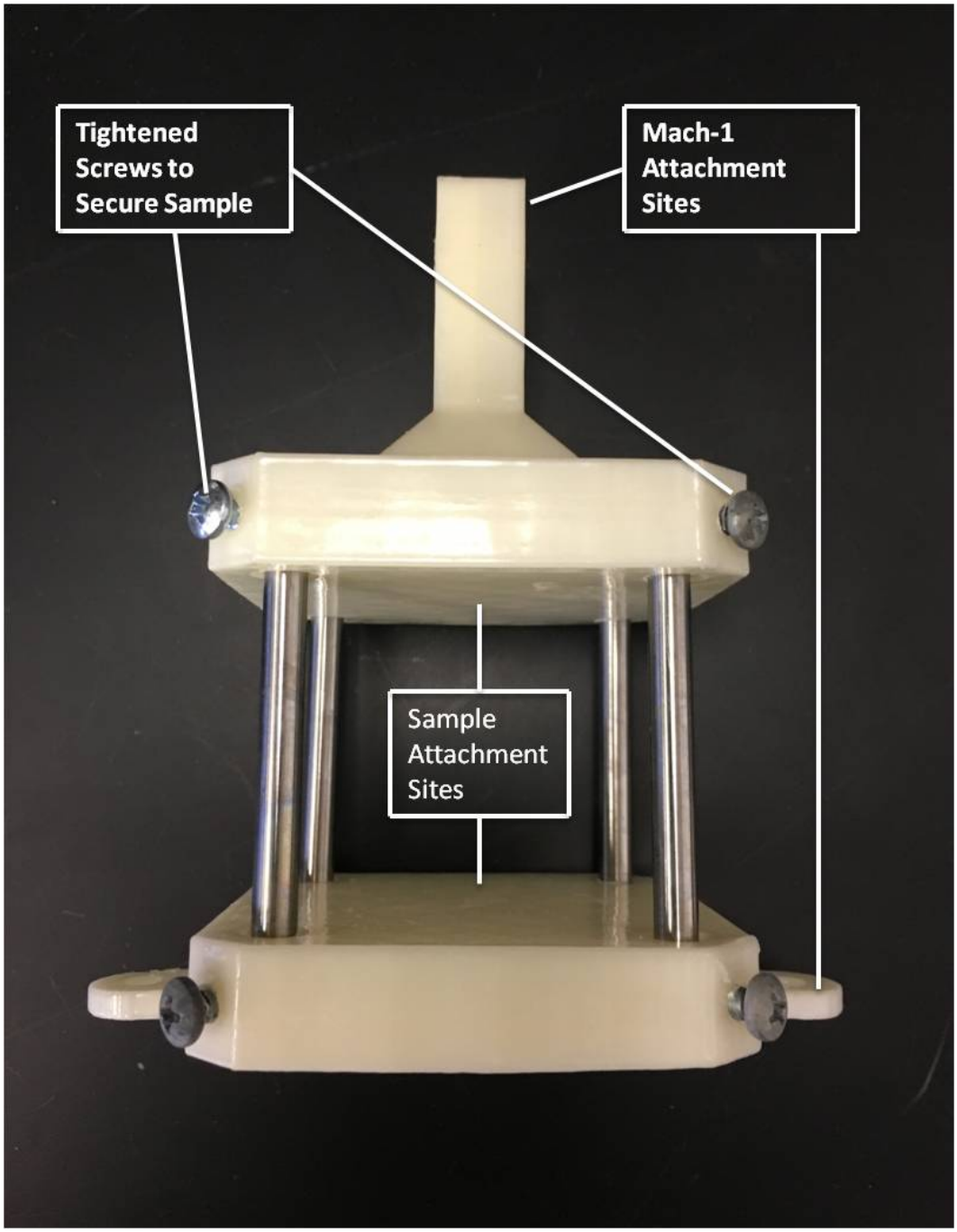

Figure 3.5 In-house customized tension attachment

3.7 Image Analysis

Using the stained images, Poisson's Ratio was used to calculate the deformations of the longitudinal and transverse cross-sections. The analysis of the cross-sections was completed using the MosaicJ plug in (Biomedical Imaging Group, Swiss Federal Institute of Technology Lausanne) with ImageJ (National Institute of Health, MD), allowing for capture of the change in dimensions at each strain level. Poisson's Ratio (ν) can be calculated using:

$$\nu = -\frac{\varepsilon lat}{\varepsilon long} \qquad 3.1$$

The sample dimension change in the longitudinal and lateral directions after testing differed between the strain levels of 15%, 30%, and 45%. For the strains tested, the change in sample dimension (Figure 3.6) from the control was calculated to ensure the same dimensional area was analyzed for histology at each strain level tested.

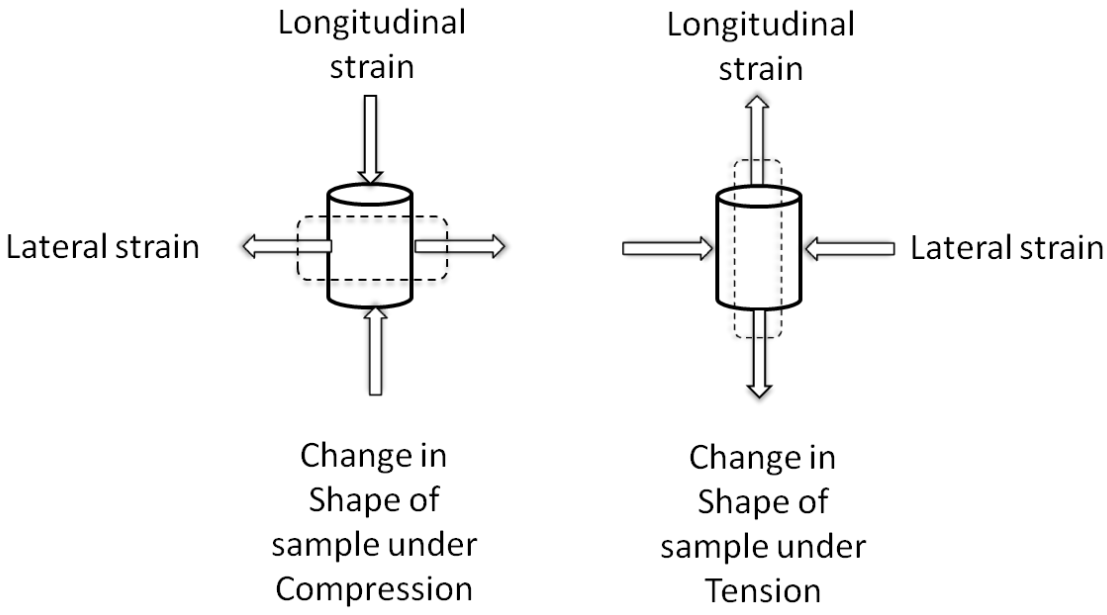

Figure 3.6 Change in sample shape after mechanical testing

The Poisson's Ratio (ν) of 0.5 was utilized to calculate the change in the dimensions of the sample during compression and tension testing for the longitudinal and transverse cross-sections. The strain level input for the test was used as the longitudinal strain to calculate the lateral strain (ε_{lat}) and the percentage of change to the samples. The value found for ε_{lat} was input into the equation as well as the original height (h) of the sample:

$$\varepsilon_{lat} = \frac{\sigma lat}{h} \qquad 3.2$$

After finding the stress (σ_{lat}), the new post-test dimensions of the fetal porcine brain sample were calculated. With the known dimension of the H & E images taken at 20x magnification with the Leica DM2500 optical microscope (Leica Microsystems Inc., Buffalo Grove, IL), the changes in the dimensions calculated were used for creating the H & E images for analysis in ImageJ.

Images of H & E slides were taken of the area on the samples after compression or tension in both the longitudinal and transverse plane (Figure 3.7).

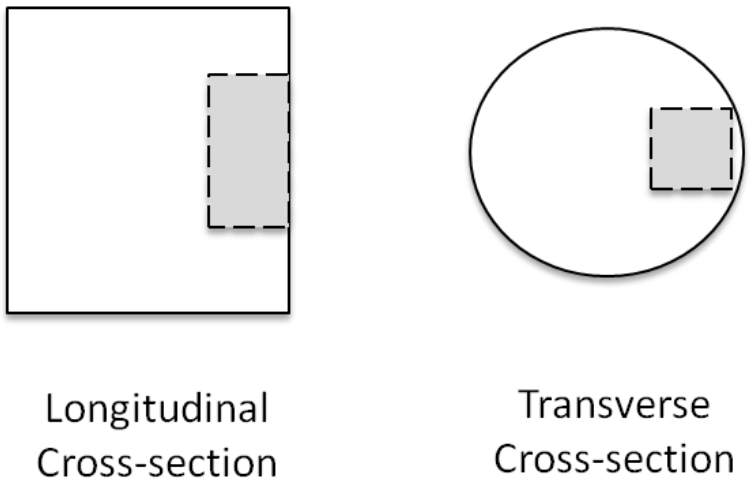

Figure 3.7 Schematic of area used on cross-sections for image analysis

Overlap on the edges of each of the images allowed them to be input into the MosaicJ plug-in and merged together to account for the change in dimension after loading at 15%, 30%, or 45% strain. The mosaic image was then imported into ImageJ and cropped to the dimensions calculated by Poisson's Ratio for each sample according to the strain level tested (Figure 3.8).

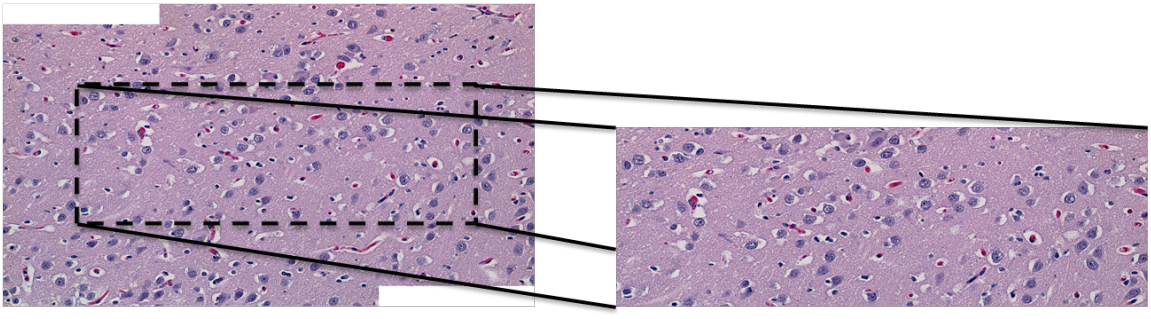

Figure 3.8 (Left) MosaicJ image of compression sample strain rate 0.00625 s^{-1} at 45% strain. (Right) ImageJ cropped MosaicJ image for analysis.

To analyze the cropped image, the blood vessels and voids were cut out of the image to ensure they were not included in the cell count. A black and white threshold image was then generated out of the cropped image for analysis (Figure 3.9). A particle analysis of the threshold image was used to output the mean area fraction (AF), percent distribution of the cells in the sample, and mean nearest neighbor distance (NND), the average distance between the cells, of each of the samples.

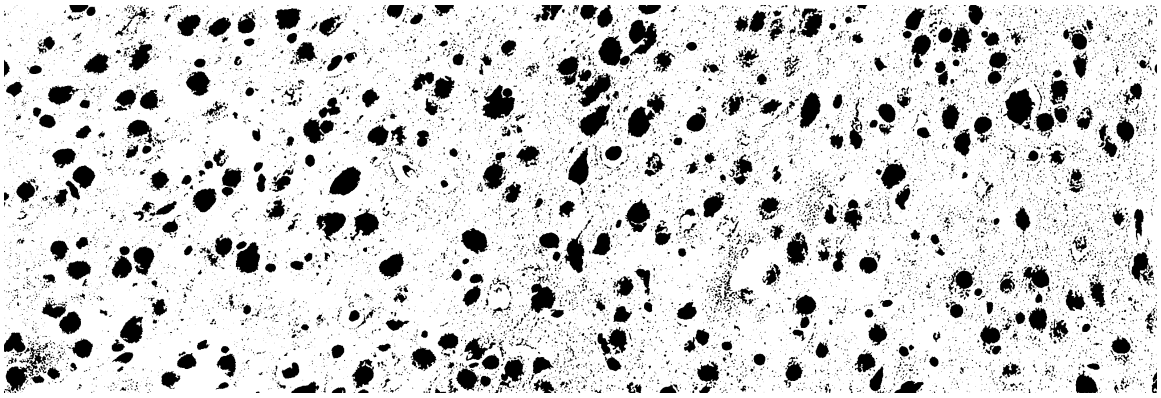

Figure 3.9 Representative black and white threshold image for a compressed sample at a strain rate of 0.00625 s^{-1} at 45% strain.

The parameters of the particle analysis included particle size, pixel units, show outlines, display results and summarize, exclude on edges, include holes, and centroid coordinates. The centroid coordinates were used in ImageJ to calculate the average nearest neighbor distance of the cells in each sample using a NND plug-in created by Yuxiong Mao.

Following the image analysis using ImageJ, with the area fraction (%) and nearest neighbor distance (μm) for each of the samples obtained, statistical analysis in Excel was used to determine if there were any statistically significant changes in the microstructure

of the fetal porcine brain samples. A comparison between the control samples and the average area fraction and nearest neighbor distance found at each strain rate tested for each strain level was conducted using a t-test to determine if there was a statistical change in microstructure with a 95% confidence interval ($t < 0.05$). A Two-Way ANOVA was also conducted using the data from every sample. The Two-Way ANOVA test compared the strain rates and strain levels tested to determine if either had a more influential effect on the microstructure of the tissue when tested. A 95% confidence interval ($p < 0.05$) was used to determine statistical significance.

CHAPTER IV

RESULTS

4.1 Mechanical Testing

4.1.1 Compression

Three strain rates were applied to samples that were loaded to strain levels of 15%, 30%, or 45% to obtain the compressive mechanical response and the corresponding imaging data required for generating structure-property relationships. Under compression, viscoelastic properties expected of brain tissue such as strain rate dependence and nonlinearity are seen in Figure 4.1. The compression curves responded with upward concavity.

The strain rate dependent behavior was described by the increase in the maximum stress level reached as the strain rate increased. In Figure 4.1, the maximum stress levels at each of the three tested strain rates to 45% strain are displayed. At the lowest strain rate of 0.00625 s^{-1} the maximum stress was 3.559 ± 0.571 kPa, the intermediate rate 0.025 s^{-1} reached 5.009 ± 0.616 kPa, and the highest rate 0.1 s^{-1} reached 9.167 ± 1.367 kPa peak stress.

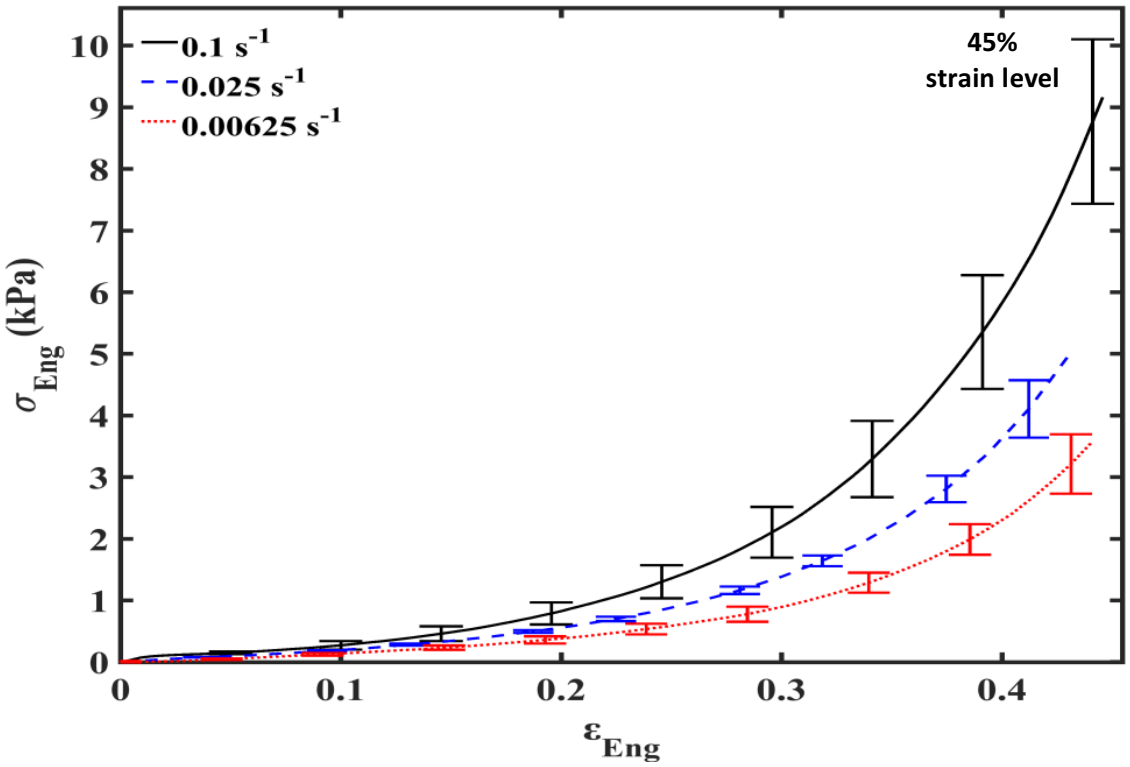

Figure 4.1 Engineering stress-strain behavior of infant porcine brain under compression.

Strain rates of 0.1 s^{-1}, 0.025 s^{-1}, and 0.00625 s^{-1} to strain level of 45%. Error bars indicate standard deviation. (n=5 each strain rate)

4.1.2 Tension

Tensile testing was conducted similarly to the compression testing on a second set of samples. The tension tests were completed with three different strain rates applied to the strain levels of 15%, 30%, and 45% when loaded to obtain the mechanical response in tension and the imaging data required for generating structure-property relationships. When samples were pulled in tension, strain rate dependency and nonlinearity was

observed as shown in Figure 4.2. The curves generated in tension were concave down instead of concave up as in compression.

The strain rate dependent behavior was described by the increase in the maximum stress level reached as the strain rate increased. Figure 4.2 shows the maximum stress reached at the lowest strain rate of 0.00625 s^{-1} was 0.174 ± 0.011 kPa, the intermediate rate of 0.025 s^{-1} reached 0.274 ± 0.032 kPa, and the highest strain rate of 0.1 s^{-1} reached 0.420 ± 0.076 kPa peak stress.

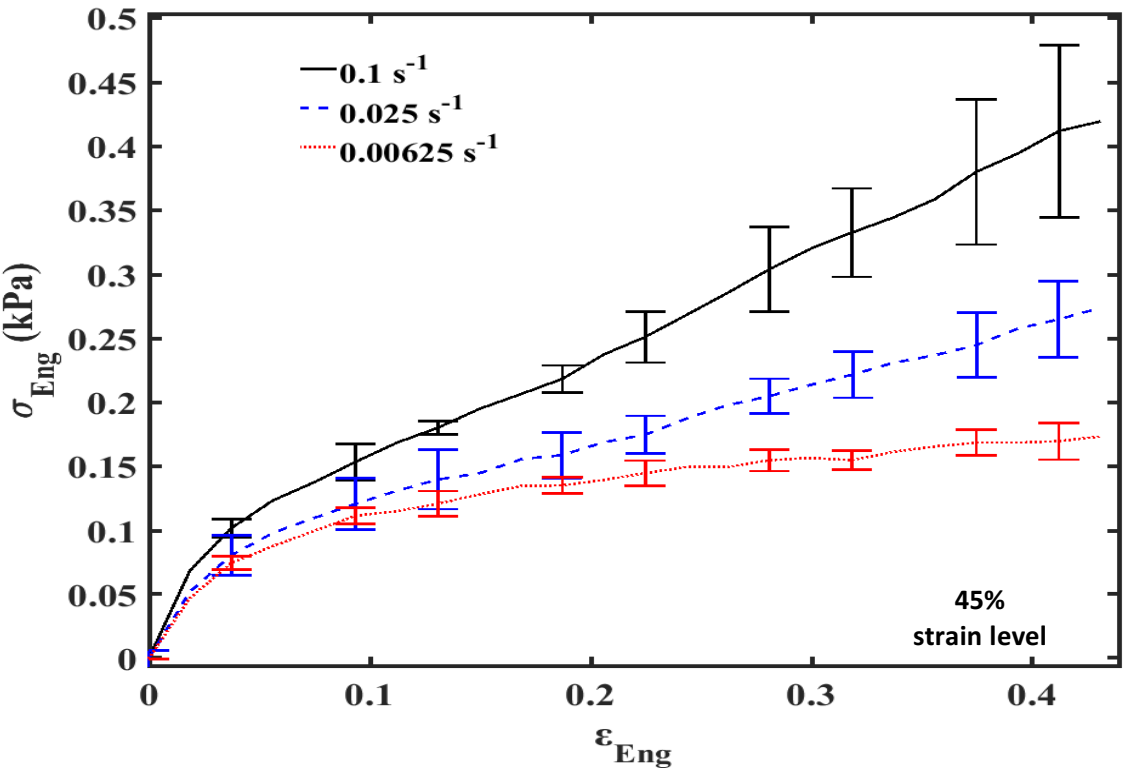

Figure 4.2 Engineering stress-strain behavior of fetal porcine brain under tensile loading.

Strain rates of 0.1 s^{-1}, 0.025 s^{-1}, and 0.00625 s^{-1} pulled to strain level of 45%. Error bars indicate standard deviation. (n=5 each strain rate)

4.2 Histology

Figure 4.3 shows a comparison of the H&E stained slides generated for samples compressed at a strain rate of 0.1 s^{-1} from control to 45% strain. A noticeable change is seen in the cell shape between the strain rate of 45% and all other strain rates tested (control, 15%, and 30%). An increase in the elongation of the neuronal cell bodies and compaction of the cells is seen most prominently at 45%. A change is less obvious in a comparison between the strain rates of control, 15%, and 30% without statistical analysis. ImageJ was used to quantify the area fraction (%), which is defined by the percent distribution of cells, and the mean nearest neighbor distance (μm), which averages the distance between neighboring cells. A statistical comparison was then conducted using a t-test and Two-Way ANOVA to determine if there was a statistically significant change to the microstructure of the tissue from control after loading at 15%, 30%, or 45% strain.

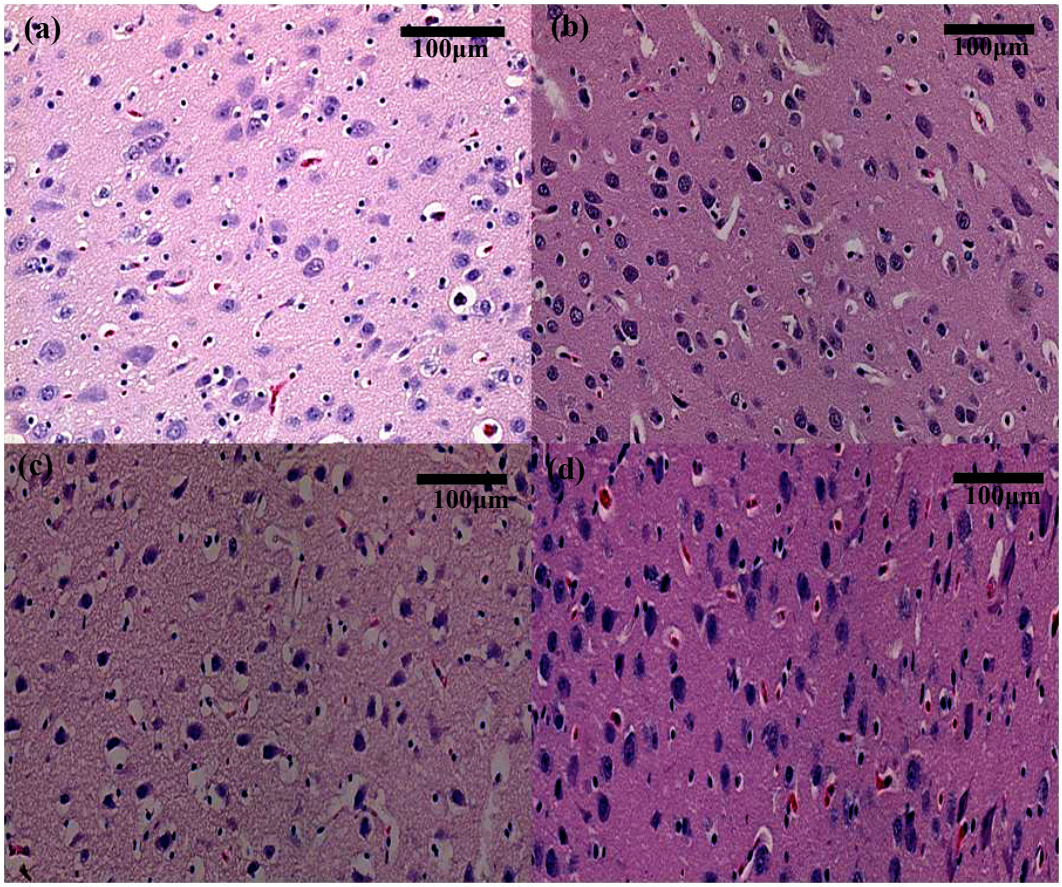

Figure 4.3 Haematoxylin & Eosin stained slides of longitudinal cross-section after compression testing.

Strain rate 0.1 s^{-1} (a) Strain level of 0% (control), (b) Strain level of 15%, (c) Strain level of 30%, and (d) Strain level of 45%. (20x magnification with 100µm scale bar)

4.2.2 Longitudinal Cross-section in Compression

Figure 4.4a shows the mean area fraction for the longitudinal cross-section following compression for the respective strain levels (control, 15%, 30%, 45%). The area fraction of the samples increased as the compression level increased while the nearest neighbor distances decreased. There is a statistically significant difference ($p < 0.05$) of strain rate 0.025 s^{-1} at strain level 30% when compared to the control group.

Additionally, all three strain rates were significantly different from the control group at a strain level of 45%. These findings indicate that the number of cells within the sample area increased with the strain level, 45% having the greatest increase in cells for all three strain rates. Using the Two-Way ANOVA, the p-values were found for both the strain rates and strain levels. The p-value ($p < 0.05$) of the strain rates was 0.807 and the p-value of the strain levels was 0.001, which indicates that the strain rate did not have statistical significance to the change in microstructure while the strain level did have a statistical significance.

Figure 4.4b shows histograms of the histological results for the mean nearest neighbor distance of the longitudinal cross-section. T-tests showed a statistical significance between the strain rate of 0.025 s^{-1} and the control at strain levels 15% and 45% along with the strain rate 0.00625 s^{-1} at 45% strain level compared to the control. These findings further validate that the cells in the sample moved closer together under compression. As with the area fraction, the nearest neighbor distance is most significant at the 45% strain level and shows the largest change in the microstructure occurred at the 45% strain level. Using the Two-Way ANOVA, the p-value ($p < 0.05$) of the strain rates was 0.114 and the p-value of the strain levels was 0.011, which shows that the strain levels had a statistical significance to the change in microstructure during loading, unlike the strain rate.

The Two-Way ANOVA test of the mean area fraction and mean nearest neighbor distance of the longitudinal cross-section after compression both showed that the strain level gave a statistically significant difference when compared to each other while the strain rate did not show a significant difference. This indicates the strain rate was not as

significant to the microstructural change of the sample as the strain levels in the longitudinal cross-section.

(a)

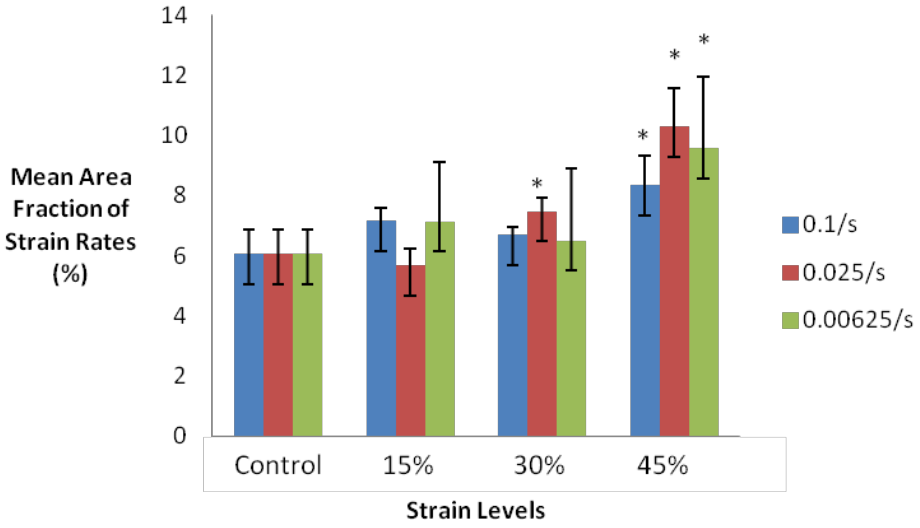

(b)

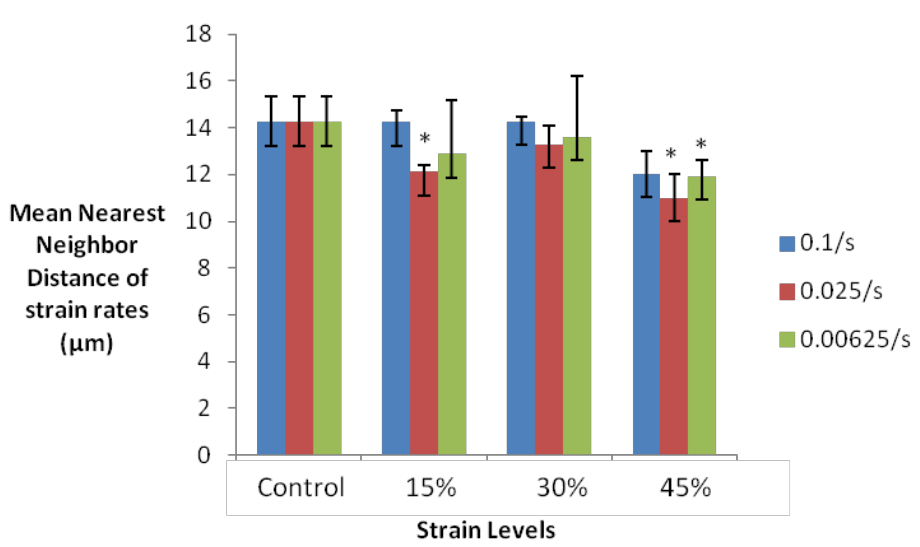

Figure 4.4 Mean (a) Area fraction and (b) Nearest neighbor distance of compressed tissue analyzed by longitudinal cross-section.

Compressed to strain levels of control, 15%, 30%, and 45% for strain rates of 0.00625 s^{-1}, 0.025 s^{-1}, and 0.1 s^{-1}. Asterisk indicates strain rate of statistical difference from the control at indicated strain level. (n=3 for each test)

4.2.3 Transverse Cross-section in Compression

Figure 4.5a shows mean area fractions of the transverse cross-section after compression. There is a statistical difference ($p < 0.05$) of the strain rates 0.025 s^{-1} and 0.00625s^{-1} at a strain level of 15% when compared to the mean area fraction of the control group. The strain rates of 0.1s^{-1} and 0.025s^{-1} are statistically different compared to the control group. Additionally, all three strain rates are significantly different from the control group at a strain level of 45%. As with the longitudinal-cross sections, the 45% strain level was significant in all three strain rates. Using the Two-Way ANOVA the p-values ($p < 0.05$) were found for both the strain rates and strain levels. The p-value of the strain rates was 0.032 and the p-value of the strain levels was 0.552, indicating the strain rate, but not the strain level, gave a statistical significance.

Figure 4.5b shows the mean nearest neighbor distance of the transverse cross-section and denotes there is a statistical significance between the strain rate of 0.00625 s^{-1} and the control at strain levels of 15% and 45%. The strain rate of 0.025 s^{-1} is also shown to be statistically different to the control at the strain level 30% and 45%. This indicates the cells were found to be closer together after compression. Using the Two-Way ANOVA, the p-values ($p < 0.05$) were found for both the strain rates and strain levels. The p-value of the strain rates was 0.001 and the p-value of the strain levels was 0.649, indicating the strain rate, but not the strain level gave a statistical significance.

The Two-Way ANOVA test of mean area fraction and mean nearest neighbor distance of the transverse cross-section after compression both gave the same result. There was a statistical significance found with respect to strain rate, however the strain level did not show a significant difference. This is the opposite finding of the results from

the longitudinal cross-section, that the strain level had the highest statistical significance. The comparison between the longitudinal and transverse cross-sections under compression shows the transverse cross-section to yield the highest instances of statistical significance.

(a)

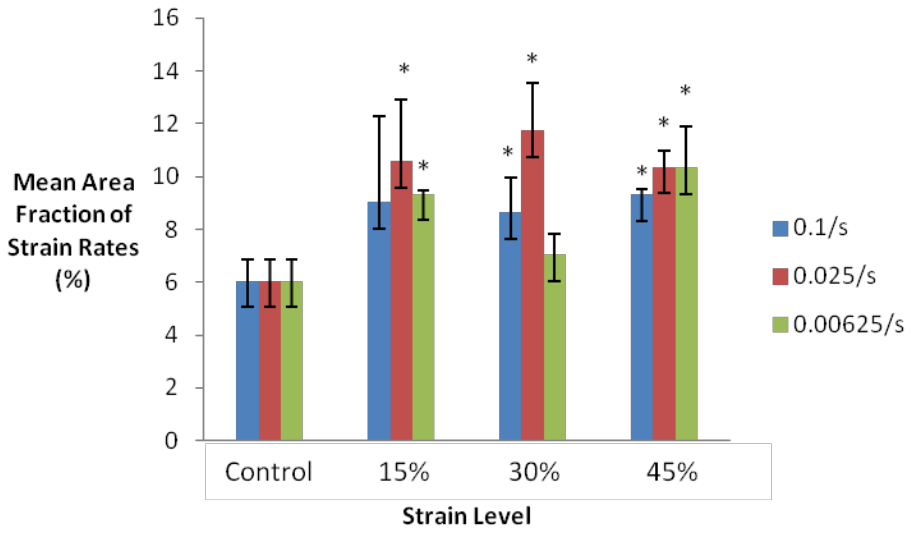

(b)

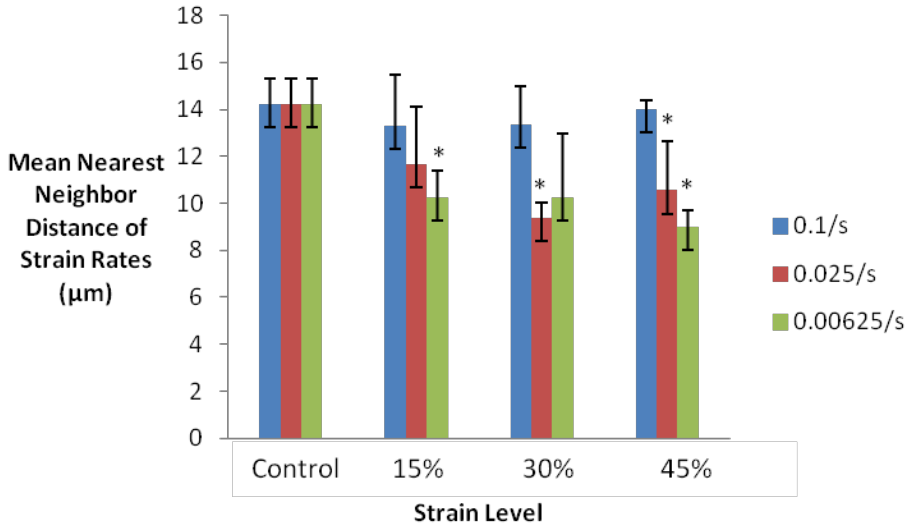

Figure 4.5 Mean (a) Area fraction and (b) Nearest neighbor distance of compressed tissue analyzed by tangential cross-section.

Compressed to strain levels of control, 15%, 30%, and 45% for strain rates of 0.00625 s^{-1}, 0.025 s^{-1}, and 0.1 s^{-1}. Asterisk indicates strain rate of statistical difference from the control at indicated strain level. (n=3 for each test)

4.2.4 Longitudinal Cross-section in Tension

Figure 4.6a shows a statistical difference ($p < 0.05$) of the strain rate 0.1 s^{-1} and 0.00625 s^{-1} at strain level 15% when compared to the mean area fraction of the control group. It also shows that all three strain rates are significantly different from the control group at a strain level of 30%. The 0.1 s^{-1} and 0.00625 s^{-1} strain rates as well are statistically significant at the 45% strain level. The statistical significances found indicate that the area fractions increased. Using the Two-Way ANOVA, the p-values ($p < 0.05$) were found for both the strain rates and strain levels. The p-value of the strain rates was 0.675 and the p-value of the strain levels was 0.944.

Figure 4.6b of the mean nearest neighbor distance shows a statistical significance between the strain rate of 0.1 s^{-1} at 15% strain level. At 30% strain level the 0.00625 s^{-1} strain rate is also statistically different than the control. The 0.025 s^{-1} and 0.00625 s^{-1} strain rates are indicated in the figure to be statistically different at the 45% strain level. The nearest neighbor distance has significance showing that the distance between the cells within the sample decreased. Using the Two-Way ANOVA, the p-values ($p < 0.05$) were found for both the strain rates and strain levels. The p-value of the strain rates was 0.141 and the p-value of the strain levels was 0.912.

A Two-Way ANOVA test that was conducted of the mean area fraction and mean nearest neighbor distance of the longitudinal cross-section after tension found there was a greater change in microstructure due to the strain rates than the strain levels tested. However, neither the strain rates nor strain levels were found to be statistically significant

to the microstructural change. No statistical significance found from the strain rate or strain level is different from the findings of the Two-Way ANOVA tests conducted on the cross-sections of the compression tests. That found the longitudinal cross-section to have a significant mictrostructural difference due to the strain level and the transverse cross-section change to be due to the strain rate.

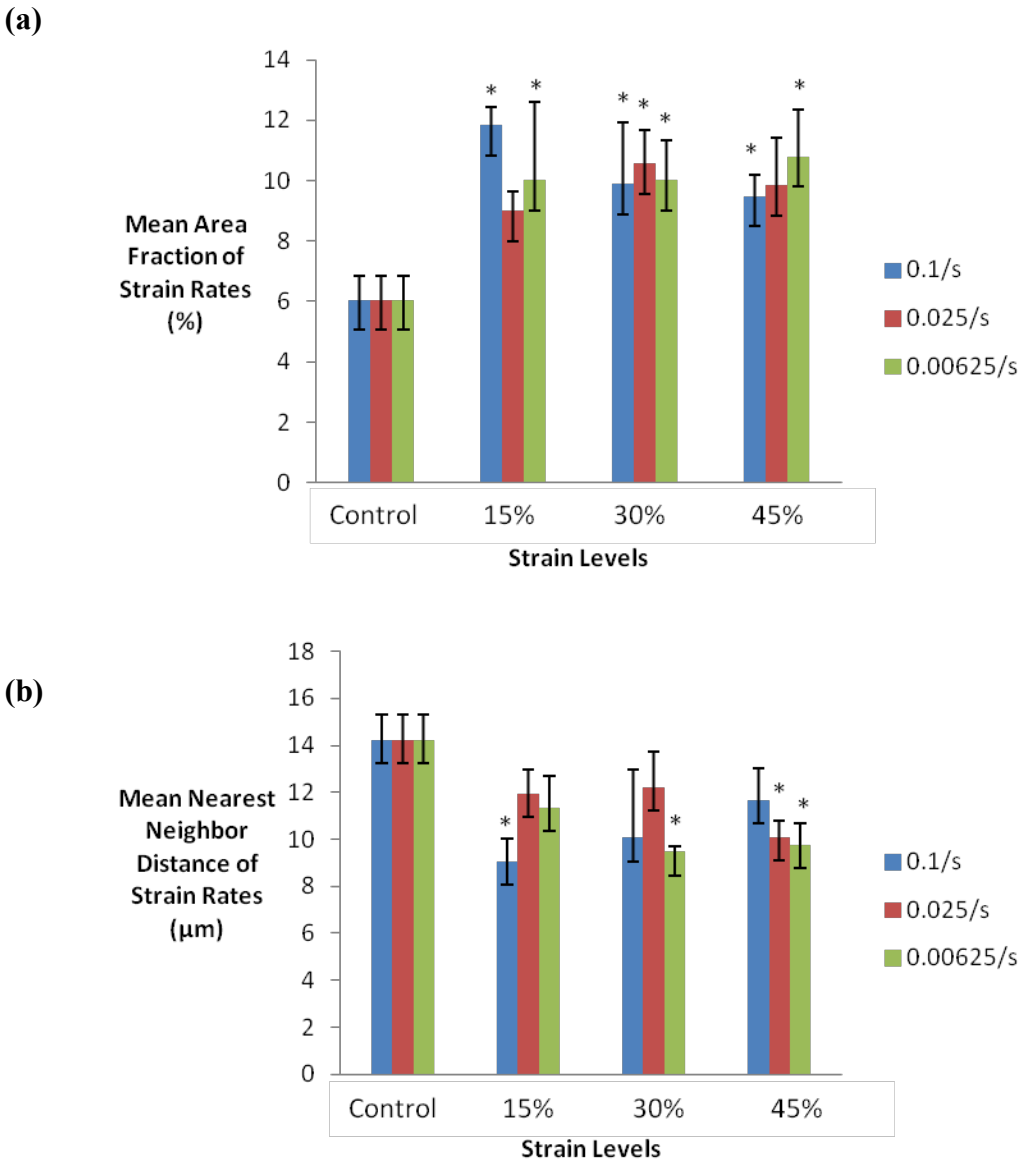

Figure 4.6 Mean (a) Area fraction and (b) Nearest neighbor distance of tensile tested tissue analyzed by longitudinal cross-section.

Tested to strain levels of control, 15%, 30%, and 45% for strain rates of 0.00625 s^{-1}, 0.025 s^{-1}, and 0.1 s^{-1}. Asterisk indicates strain rate of statistical difference from the control at indicated strain level. (n=3 for each test)

4.2.5 Transverse Cross-section in Tension

Figure 4.7a shows there is a statistical difference ($p < 0.05$) of the strain rate 0.00625 s^{-1} at strain level 15% when compared to the mean area fraction of the control group. It also shows that there is a statistical difference of the strain rate 0.1 s^{-1} at strain level 30% when compared to the mean area fraction of the control group. The significant tests indicate the number of cells increased in the tissue. Using the Two-Way ANOVA, the p-values ($p < 0.05$) were found for both the strain rates and strain levels. The p-value of the strain rates was 0.788 and the p-value of the strain levels was 0.583.

Figure 4.7b shows a statistical significance between none of the strain levels when compared to the control. The figure, while appearing to show there was a decrease in the mean nearest neighbor distance, did not have a large enough decrease in distance to be a statistically significant change. Using the Two-Way ANOVA, the p-values ($p < 0.05$) were found for both the strain rates and strain levels. The p-value of the strain rates was 0.956 and the p-value of the strain levels was 0.629, denoting no significant difference.

The Two-Way ANOVA test conducted of the mean area fraction and mean nearest neighbor distance of the transverse cross-section after tension found there was a greater change in the microstructure due to the strain levels than the strain rates tested, which is the opposite finding of the longitudinal cross-section in tension. Though, neither the strain rates nor strain levels were found to be statistically significant to the microstructural change after testing. No statistical significance found from the strain rate or strain level is the same finding as the Two-Way ANOVA result of the longitudinal cross-section under tension.

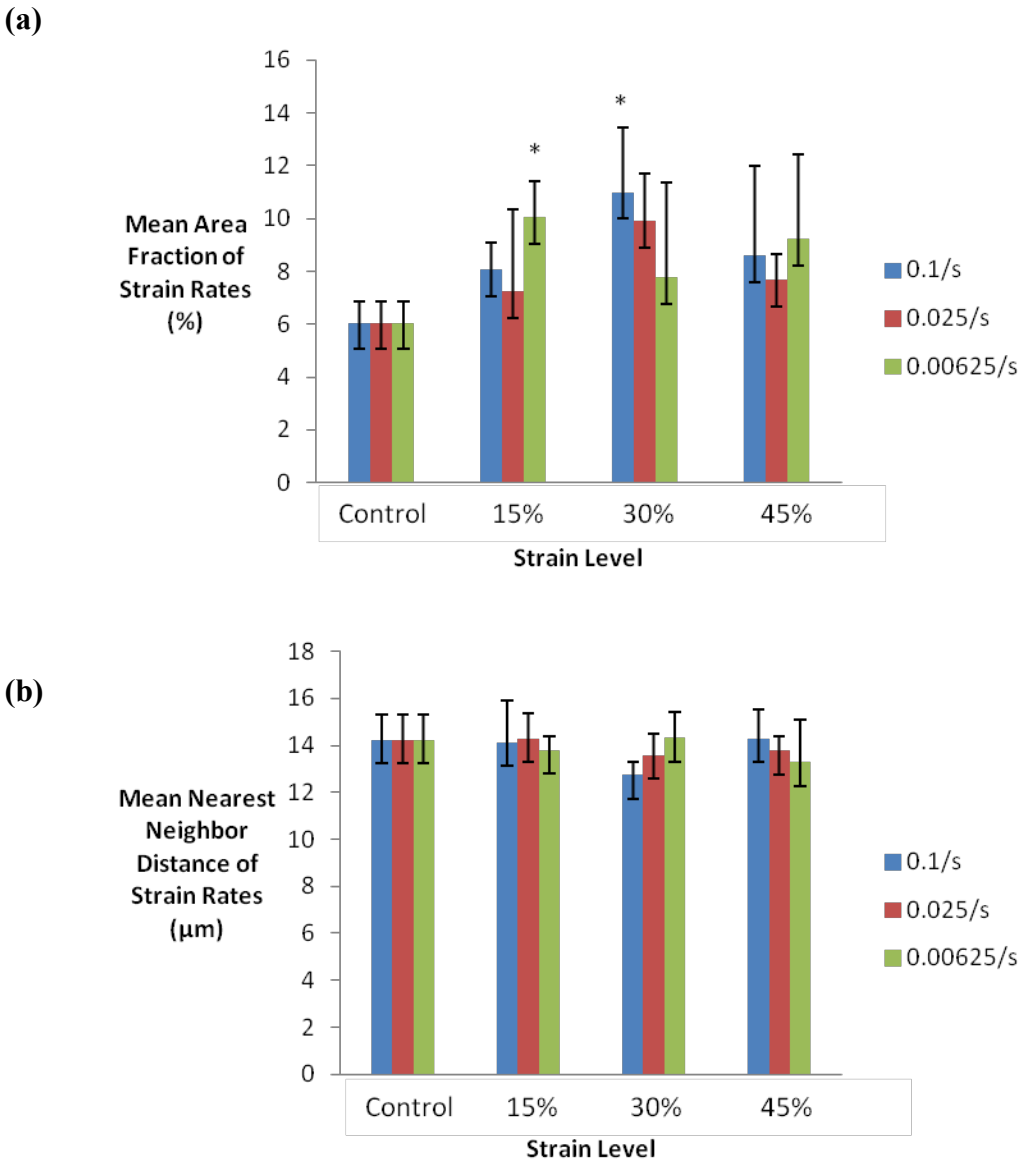

Figure 4.7 Mean (a) Area fraction and (b) Nearest neighbor distance of tensile tested tissue analyzed by tangential cross-section.

Tested at strain levels of control, 15%, 30%, and 45% for strain rates of 0.00625 s^{-1}, 0.025 s^{-1}, and 0.1 s^{-1}. Asterisk indicates strain rate of statistical difference from the control at indicated strain level. (n=3 for each test)

4.2.6 Total Area of Cells

A quantification of the mean percent area fraction found during image analysis of the longitudinal and transverse cross-sections under compressive and tensile loading was

found by multiplying the area fraction and cell size, which is generated by ImageJ using the number of pixels the cell area covered converted to μm^2 (Table 4.1).

$$\text{Total Area of the Cells} = \text{Area Fraction (\%)} \times \text{Cell Size } (\mu m^2) \qquad 4.1$$

In Figure 4.8 a linear trend line was fit to the total cell areas found at strain rate 0.1 s^{-1} from control to 45% strain. The control value of the cell area in the longitudinal and transverse cross-sections was 1194.470 ± 46.611 μm^2 and 1452.716 ± 77.103 μm^2 respectively. In transverse compression the cell area increased to 2172.992 ± 52.978 μm^2 at 15% strain, before reducing to 2040.378 ± 128.748 μm^2 at 30% strain and rising to 24.77.702 ± 114.123 μm^2 at 45% strain. The changes of the transverse cross-section under tension resulted in an increase at 15% strain to 1823.212 ± 245.072 μm^2. The cell area also increased at 30% strain to 2492.211 ± 300.023 μm^2 before decreasing to 2083.972 ± 447.071 μm^2 at 45% strain. Under tensile loading the longitudinal cross-section also increased from control at 15% strain to 1673.436 ± 120.253 μm^2, before decreasing at 30% strain to 1466.871 ± 314.655 μm^2. The total cell area increased again at 45% strain to 1927.119 ± 140.123 μm^2. The longitudinal cross-section under compression resulted in the same trend between the strain levels (control, 15%, 30%, 45%) as the transverse cross-section. At 15% strain the cell area increased to 1659.703 ± 97.321 μm^2, 30% strain decreased to 1349.848 ± 60.491 μm^2, and 45% strain increased to 1602.117 ± 247.351 μm^2. The trend lines fit to these total cell areas show an increase in the total area of the cells as the strain level increased from control to 45% strain under compressive and tensile loading in both the longitudinal and transverse cross-sections.

Table 4.1 Total cell area (μm^2) of cross-sections at strain rate 0.1 s^{-1} from control to 45% strain. (n=3 for each condition)

Cross-Section Conditions	Control (0%) Strain	15% Strain	30% Strain	45% Strain
Longitudinal Compression	1194.470 ± 46.611	1659.703 ± 97.321	1349.848 ± 60.491	1602.117 ± 247.351
Transverse Compression	1452.716 ± 77.103	2172.992 ± 52.978	2040.378 ± 128.748	24.77.702 ± 114.123
Longitudinal Tension	1194.470 ± 46.611	1673.436 ± 120.253	1466.871 ± 314.655	1927.119 ± 140.123
Transverse Tension	1452.716 ± 77.103	1823.212 ± 245.072	2492.211 ± 300.023	2083.972 ± 447.071

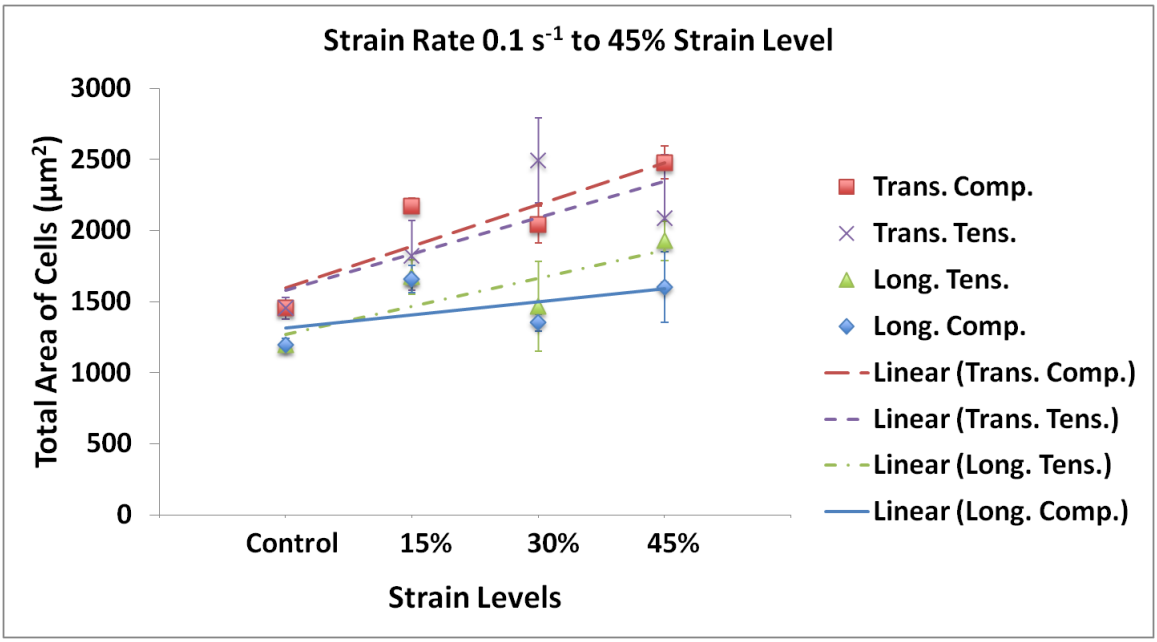

Figure 4.8 Total area of cells in tissue at 0.1 s^{-1} strain rate to 45% strain longitudinal and transverse cross-sections under compressive and tensile loading. Linear trend lines. (n=3 for each test)

4.2.7 Cell Deformation

The cell deformation captured by image analysis was further quantified by multiplying the area fraction and nearest neighbor distance to find the amount of change in the cell shape.

$$\text{Cell Deformation} = \text{Area Fraction (\%)} \times \text{Nearest Neighbor Distance (μm)} \quad 4.2$$

The longitudinal and transverse cross-sections of both compression and tension from control to 45% strain were compared for strain rate 0.1 s^{-1} to determine any trends (Figure 4.9). The control value of the cells in the longitudinal and transverse cross-sections respectively was 86.03 μm and 95.67 μm. At 45% strain the transverse tension cross-section had a cell deformation value of 122.65 μm, transverse compression had a value of 130.21 μm, longitudinal tension had a value of 110.59 μm, and longitudinal compression had a value of 100.24 μm. The linear trend lines, when fit to the graph, show an increase in deformation from the control samples for the longitudinal and transverse cross-sections of both compressive and tensile testing. The transverse tension data has an outlier at 30% strain of 139.85 μm. There is reason to believe there were inconsistencies with the data acquisition at 30% strain as the damage found in transverse tension was higher at the 30% strain level than at 45% strain.

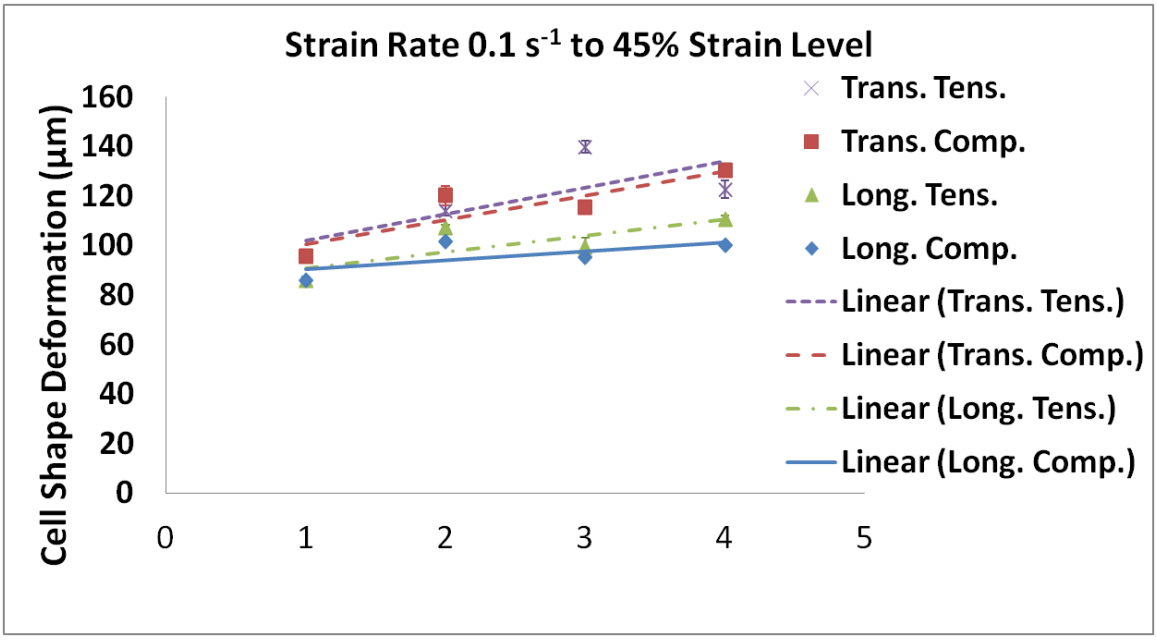

Figure 4.9 Cell shape deformation at 0.1 s^{-1} strain rate to 45% strain longitudinal and transverse cross-sections under compressive and tensile loading. Linear trend lines. (n=3 for each test)

CHAPTER V

DISCUSSION

5.1 Validation of Using Porcine Specimens

Porcine specimens are often used as substitutes for humans in both adult and infant brain testing.[3,4,11,12,14,18] The porcine brain is used for its similarity to the human brain including the shape and the presence of the sulci and gyri as opposed to rodent brains.[2] Developmentally, the fetal porcine brain is further along than a human infant's with a greater amount of myelination present indicating neuronal maturity. Dobbing et al. used brain mass growth rate over the first decade of a humans' life, to determine that months of development in a human is roughly equaled to weeks of development in a pig.[5,6] This developmental scale was supported by Thibault et al. using a physiological analysis and comparison of Dobbing's findings.[14] Using stillborn fetal piglets gives the opportunity for mechanical and histological data equivalent to a human child under one month old allowing for understanding of TBI from the earliest developmental stages after birth.

5.2 Interpretation of Data

5.2.1 Analysis of Mechanical Testing in Compression

Typical responses of viscoelastic soft tissues were observed in the compression testing of the infant brain tissue. Strain rate dependency and nonlinearity was seen in Figure 4.1 at strain rates 0.00625 s^{-1}, 0.025 s^{-1}, and 0.1 s^{-1} when tested to 45% strain. The

strain rate dependency could be attributed to the neurons, glial cells, and fluid contained in the tissue when compressed not having the time to adjust to the load. The tissue being compressed under physiological conditions within the PBS bath keeps the tissue hydrated and keeps liquid inside the lobes of the tissue. When the tissue was compressed, less time was allowed for the liquid to move out of the tissue and for the cells to move as the cells were forced closer together toward the middle of the sample.

Non-linearity is illustrated in the compressive stress state under quasi-static testing as a concave up graph as shown in Figure 4.1. The increasing slope of the curve results from the increase in stress state as the sample is forced to compact, creating a need for more force to load the sample.

5.2.2 Analysis of Mechanical Testing in Tension

Strain rate dependency was seen in Figure 4.2 with the three strain rates (0.00625 s^{-1}, 0.025 s^{-1}, and 0.1 s^{-1}) tested to 45% strain. Rate dependency may be attributed to the cells and fluid in the tissue when tensile loaded not having the time to adjust to the load applied causing a higher stress state as the tissue is tested at higher rates. The neurons and glial cells forced to rearrange and the extracellular fluid forced out of the tissue created an increasing stress as the strain rate increased. The tension test was not conducted in a PBS bath; however, the samples were kept hydrated before testing using PBS.

The tensile stress state under quasi-static testing is concave down as shown in Figure 4.2. The decreasing slope occurs from the stress state decreasing as possible micro-tears occur within the tissue during loading. Micro-tears will reduce the amount of force necessary to pull in tension.

The unconfined tensile loading (Figure 4.2) was found to result in lower stress levels than the unconfined compressive loading (Figure 4.1) under all strain rates tested. The difference in stress levels between the stress states could result from the difference in load required to test each stress state. In tension, the weak extracellular matrix surrounding the glial cells and neuronal cell bodies allow for easier movement of the cells away from each other when pulled in tension. In compression, the cells create higher stress when forced together and into an elongated shape within the aqueous environment. The difference in stress level could also be aided by the compression test being conducted in a PBS bath while the tension testing was not.

5.2.3 Histological Analysis of Longitudinal Cross-Section Under Compression

When tissue is compressed the tissue is forced into a more compact shape along the y-axis. The compaction of the tissue forces the neurons and glial cells within to be forced from a rounded shape into a more elliptical shape, elongated in the positive and negative directions along the x-axis (Figure 5.1). During compressive loading, when the cells are elongating, fluid in the tissue is forced out by the compressive force on the tissue and the cells move toward the midline of the sample at the x-axis.

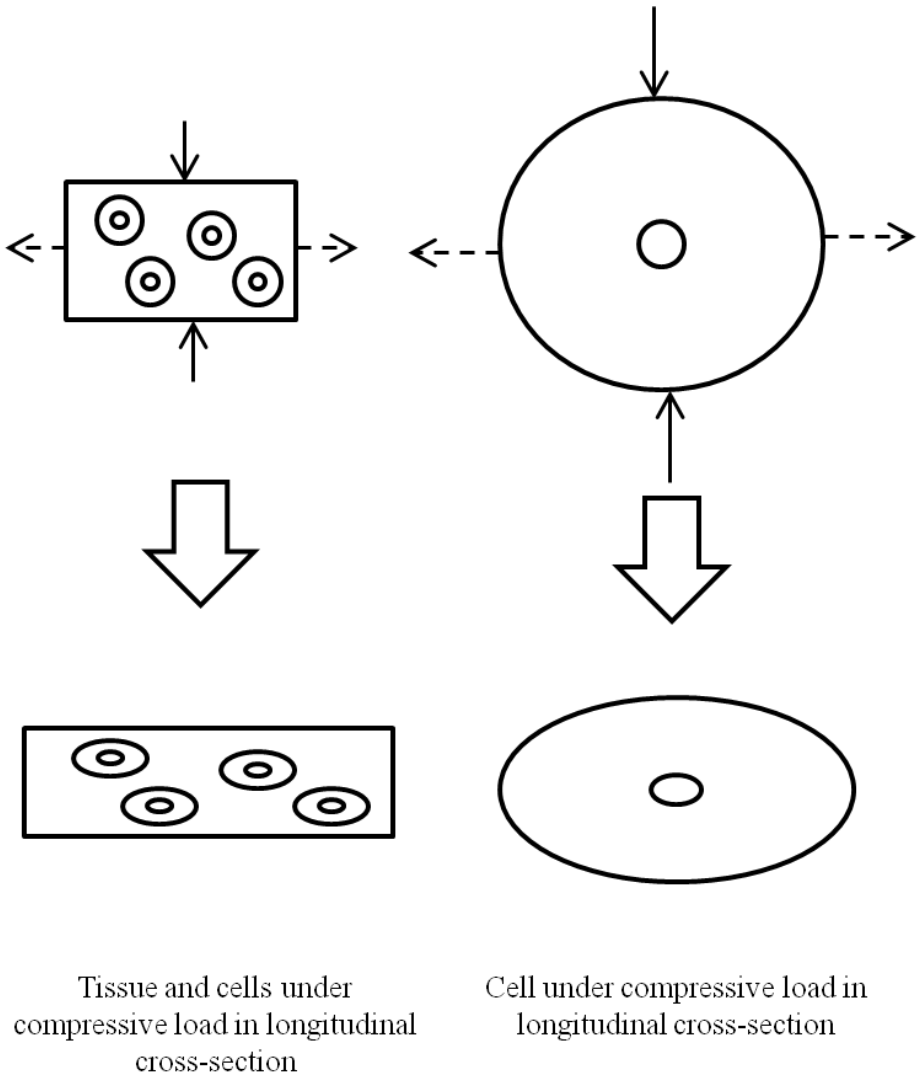

Figure 5.1 Schematic of tissue and cell deformation under compressive loading within the longitudinal cross-section. Solid arrows indicate loading direction and dashed arrows indicate tissue/cell movement direction.

The change in shape and location of the cells within the tissue was analyzed using the mean area fraction and mean nearest neighbor distance. The expected finding is an increase in mean area fraction and decrease in mean nearest neighbor distance in the longitudinal cross-section after compressive loading. Figure 4.4 shows an increase in the mean area fraction from the control with the most significant elevation in area fraction

happening at 45% strain. The mean area fraction increased as the elongation of the cells became larger. The mean nearest neighbor distance shows a decrease from the control value with its most significant change also at 45% strain. The decrease in mean nearest neighbor distance of the cells in the tissue was caused by the movement of the elongated cells closer together toward the midline of the y-axis. Loss of fluid within the tissue and the outward radial movement of the tissue during compression allowed for this closer compaction of the cells within the tissue.

A Two-Way ANOVA was conducted to determine if the strain rates or strain levels tested had a larger impact on the mean area fraction and mean nearest neighbor distance. The strain rate was found to not have as great a significance to the change in microstructure when compared to the strain level, supported by the 45% strain level having the most statistical changes in mean area fraction and mean nearest neighbor distance from control. The finding indicates the amount of compression of the tissue had a larger effect on the microstructural change in the longitudinal cross-section than the rate at which the load was applied. The tissue was compressed in the negative direction along the y-axis and the amount of compressed stress received by the tissue would alter the tissue's structure in this plane the most.

5.2.4 Histological Analysis of Transverse Cross-Section Under Compression

Under compressive loading, when looking at the transverse cross-section, cells are expected to have elongated as within the longitudinal cross-section. The cells as they are elongating, move outward radially in the tissue with the expansion of the tissue sample in all directions equally (Figure 5.2).

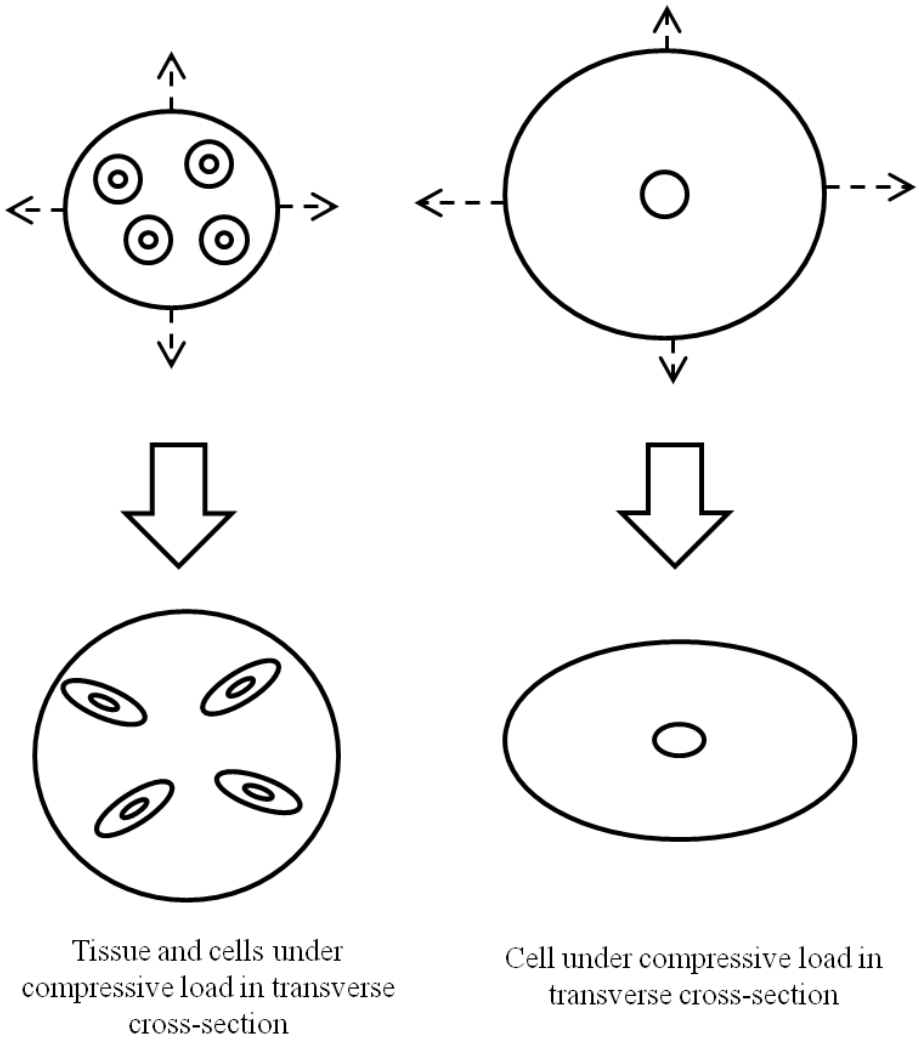

Figure 5.2 Schematic of tissue and cell deformation under compressive loading within the transverse cross-section. Solid arrows indicate loading direction and dashed arrows indicate tissue/cell movement direction.

An increased mean area fraction is expected from the elongation of the cells and an increase in size from being compressed in the negative direction on the y-axis. The mean nearest neighbor distance is expected to increase with the cells moving away from each other during radial expansion of the tissue. Comparison of the expected findings to the mean area fraction and mean nearest neighbor distance in Figure 4.5, the mean area

fraction is shown to increase from the control values. The mean nearest neighbor distance contrary to expected shows a decrease from the control values found. A barreling of the tissue, from the platen not containing a non-stick surface, during compression would have caused the cells to move outward radially as well as inward to the middle of the sample. The barreling would cause the cells within the tissue to undergo outward radial movement along the outer edge, as well as radial movement inward toward the middle of the sample for the inner cells. An additional factor in the difference between the expected and found mean area fraction and mean nearest neighbor distance could be the analyzed image being taken at the edge of the sample causing an edge effect that would not be seen in the middle of the sample.

The Two-Way ANOVA was used to compare the mechanical testing parameters of the strain rate and strain level to the area fraction and nearest neighbor distance quantified during image analysis. The finding of the Two-Way ANOVA was the strain rate created a larger statistically significant change in the microstructure than the strain level. The finding indicates the rate at which the tissue was forced to compress and the tissue was forced to move outward radially during compression had a larger effect on the microstructure than the amount the sample was compressed to. The tissue would have less time to adjust outward under the load as the sample was compressed, making the strain rate important to the microstructural change.

5.2.5 Histological Analysis of Longitudinal Cross-Section Under Tension

When pulled in tension the tissue elongates in the direction of loading, while the tissue moves radially inward from all directions. The upward pulling of the tissue causes an elongation of the cells in the same direction during testing (Figure 5.3).

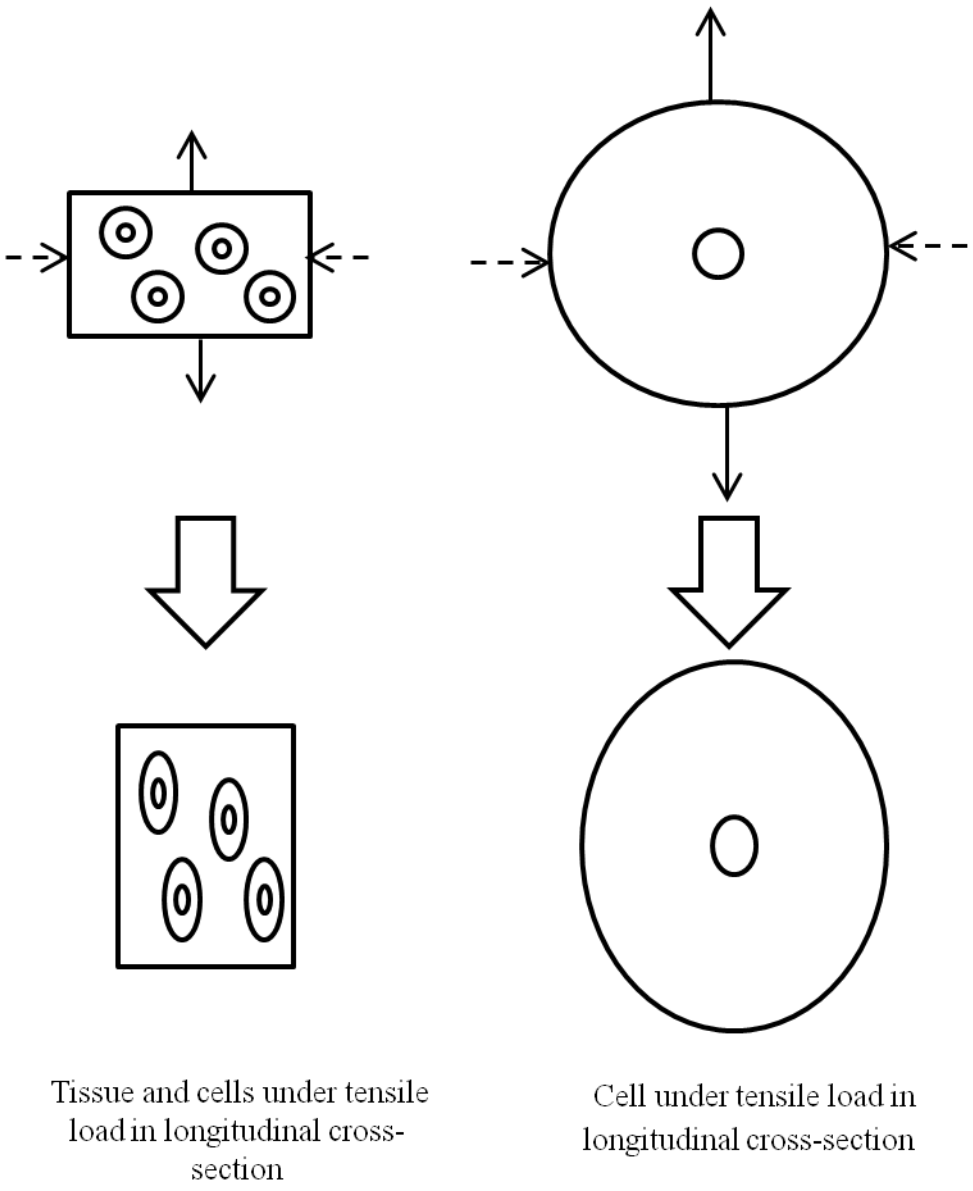

Figure 5.3 Schematic of tissue and cell deformation under tensile loading within the longitudinal cross-section. Solid arrows indicate loading direction and dashed arrows indicate tissue/cell movement direction.

The area fraction is expected to increase, while the nearest neighbor distance is expected to increase as well. The area fraction increase is due to the elongation of the

cells within the tissue as a result of the positive movement of the top of the sample. The nearest neighbor distance is expected to increase due to the movement of the cells toward the top and bottom of the tissue during tensile loading. The movement of the cells away from each other toward the top and bottom of the sample would cause separation of the cells at the middle of the sample along the x-axis providing a larger mean nearest neighbor distance.

A comparison of the longitudinal cross-section under tension in Figure 4.6, shows an increase in the mean area fraction from the control sample after testing and decrease in the mean nearest neighbor distance. The elongation of the cells during tension in the longitudinal plane and the radial movement inward caused an increased mean area fraction. As the tissue comes closer together during inward radial movement, the elongated cells move closer together and the fluid in the tissue is forced out creating a denser cellular configuration, a decreased mean nearest neighbor distance. The difference in outcome from expected of the mean nearest neighbor distance could be a result of the sample being secured to the tension attachment by glue. The tissue is not able to move at the attachment sites creating a bowing in the middle of the sample as apposed to straight sides. The cells within the tissue would move inward radially from the edge of the sample and outward radially from the middle of the sample. Taking the analysis of the image from the edge of the sample, as was done in this study, could have caused edge effect also affecting the outcome and attributing to the difference in result than expected.

The Two-Way ANOVA test found that there was no statistical significance to the change in microstructure of the samples due to the strain rate or strain levels when the samples were mechanically tested. While no statistical significance was found, the strain

rate was calculated to be more significant than the strain level. The rate the tissue is forced apart influences how long the tissue has to adjust to the change in strain level. Brain tissue is less resistant to tensile loading than compressive loading, as the weak neuronal pathways within the glial cells are easier to force apart than to compress.

5.2.6 Histological Analysis of Transverse Cross-Section Under Tension

In the transverse cross-section, the tissue and cells move inward radially while pulled in tension and the cell diameter becomes smaller. The decreased diameter results from the elongation of the cell in the positive and negative directions along the y-axis in the longitudinal plane (Figure 5.4).

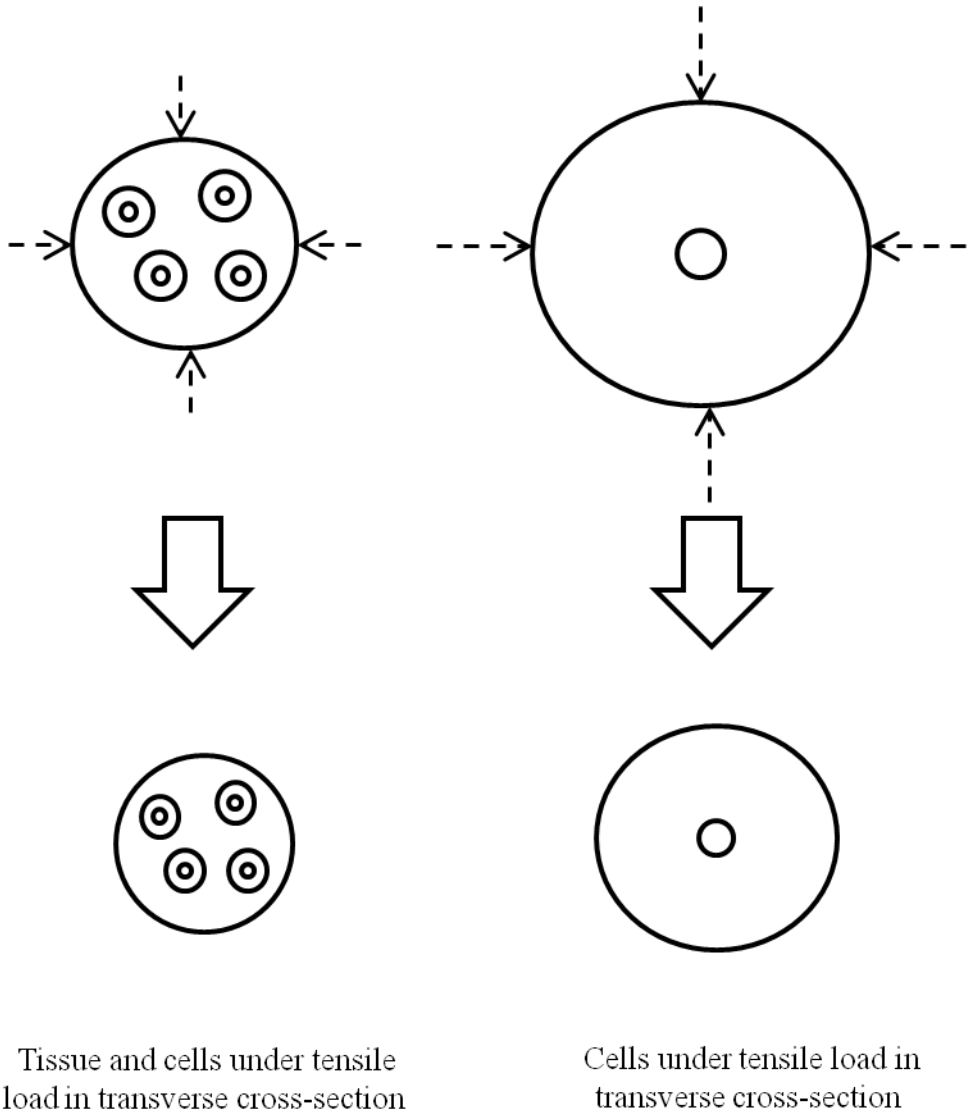

Figure 5.4 Schematic of tissue and cell deformation under tensile loading within the transverse cross-section. Solid arrows indicate loading direction and dashed arrows indicate tissue/cell movement direction.

The mean area fraction of the sample when analyzed is expected to increase and mean nearest neighbor distance is expected to decrease. The expected increase in mean area fraction is a result of a greater density of cells within the image area analyzed after

the cells are moved inward radially. The mean nearest neighbor distance is expected to decrease with the radial movement of the cells, as they are forced closer together.

Comparing the mean area fraction and mean nearest neighbor distance of the transverse cross-section under tension (Figure 4.7) shows a change in the mean area fraction of the samples compared to the control with two statistically significant increases. The mean nearest neighbor distance showed some decrease from control, however, no statistically significant decreases were found. The increase in mean area fraction is due to the increase of cells within the tissue area analyzed along the edge of the tissue. A statistically constant mean nearest neighbor distance is produced when the distance between the increased number of smaller diameter cells is analyzed after moving closer together.

As with the longitudinal cross-section, the Two-Way ANOVA test found that neither the strain rate or strain level had a statistical significance to the change in microstructure of the samples when mechanically tested. Although no statistical significance was found, the strain level was statistically more influential to the change in cell morphology in the transverse cross-section under tensile loading. The amount of change in the diameter of the tissue is reliant on the change in height of the sample, determined by the strain level and giving it more influence in the transverse cross-section.

5.2.7 Total Area of Cells in the Tissue

The total area of the cells was calculated for the quantification of the percent areas found using ImageJ. The change in cell shape and density of cells within the analyzed sample area gave an increased mean total area of the cells from the control values after loading at all strain levels (15%, 30%, 45%) (Table 4.1). Figure 4.8 shows linear trend

lines fit to the mean total cell areas calculated that illustrate an increasing mean total cell area with the increasing strain levels to 45%.

A comparison of the mean percent area fractions and mean total area of the cells after compressive or tensile loading at strain rate 0.1 s^{-1} to 45% strain gives the same trend, with the exception of longitudinal tension at 45%. All values from the loaded tissue had higher mean area fractions and mean total cell areas than the control values. In longitudinal and transverse compression both the mean area fraction and mean cell area increased at 15%, decreased at 30%, and increased again at 45% strain. The trend for longitudinal tension is an increase from control in the mean area fraction and mean total cell area at 15% strain and decrease in both at 30% strain. At 45% strain the mean area fraction decreased from its 30% strain value, while the mean total cell area increased. The transverse tension cross-section had an increased mean area fraction and mean nearest neighbor distance after 15% strain and after 30% strain. The increase between the 15% and 30% strains is disparate from the findings of the compression and longitudinal tension cross-sections. The inconsistency can be seen in Figure 4.7 as an outlier in the trend of the 30% strain levels decreasing from the values of the 15% strain. The 45% strain values for mean area fraction and mean total area of cells were also inconsistent with the findings of the trend for the 45% strain level to increase. The total area of the cells within the tissue samples was only one way the local change in morphology after loading was analyzed.

5.2.8 Cell Deformation

An additional look at the local change in cells was taken using the quantification of cell deformation to understand the change in cell morphology. The linear trend lines of

the analysis of cell deformation in Figure 4.9 show an increase change in the cell morphology from the control as the strain level increases to 45%. A comparison of the trend line in the transverse cross-sections of the compression and tension tests found the cell deformation after tension testing to be a more significant change in the cells than compression. The longitudinal cross-sections, which had lower cell shape variation at control than the transverse cross-section, also had a higher cell deformation after tension testing than compression testing. The larger cell deformation found after tension in both the longitudinal and transverse cross-sections indicates that the cells elongated and moved closer together during tensile testing more than compression. Another similarity between the deformations is the longitudinal cross-sections have less cell-deformation than the transverse cross-section for both compression and tension testing. The radial movement of the cells outward during compression and inward during tension is indicated to cause a greater change in cell morphology than occurs in the longitudinal plane during load.

5.3 Comparison of Existing Research

It has been found that there is a difference in the results found after mechanical testing when adult and infant results are compared.[14,16] Comparison of adult porcine brain by Begonia et al. with the data from this study, Figure 5.1a and Figure 5.1b, show that there is a similar trend in compression testing of brain.[1] A similar non-linear response is seen in both figures with a positive slope. Compression results from both the adult and fetal pigs show the strain rate dependent response expected of viscoelastic soft tissue such as the brain. The stresses reached during compression of the tissues lead to differing results between adult and fetal samples.

The stress level reached when the adult porcine brain was mechanically compressed at all three strain rates tested was lower than the stress level reached when the fetal porcine brain was compressed to the same strain level of 40%. The max stresses of the adult data were 1.584 kPa at 0.00625 s^{-1}, 1.724 kPa at 0.025 s^{-1}, and 3.009 kPa at 0.1 s^{-1}. For the fetal data, the max stresses were 2.390 kPa at the lowest strain rate, 3.380 kPa at the intermediate strain, and 5.840 kPa at the highest strain rate.

The higher stress levels reached in the fetal porcine brain during compression testing may be due to the larger amount of fluid in the tissue of the fetal brain as compared to the adult brain. Water is known to be incompressible, so a more aqueous environment along with the globular glial cells making up a more significant amount of the brain's structural integrity may explain the increase in stress level under compression of the fetal porcine brain.

(a)

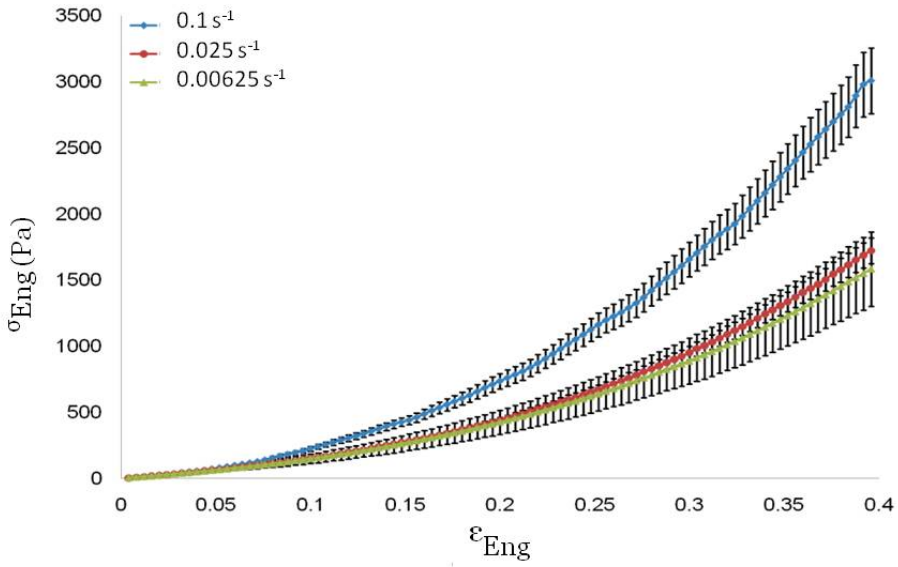

(b)

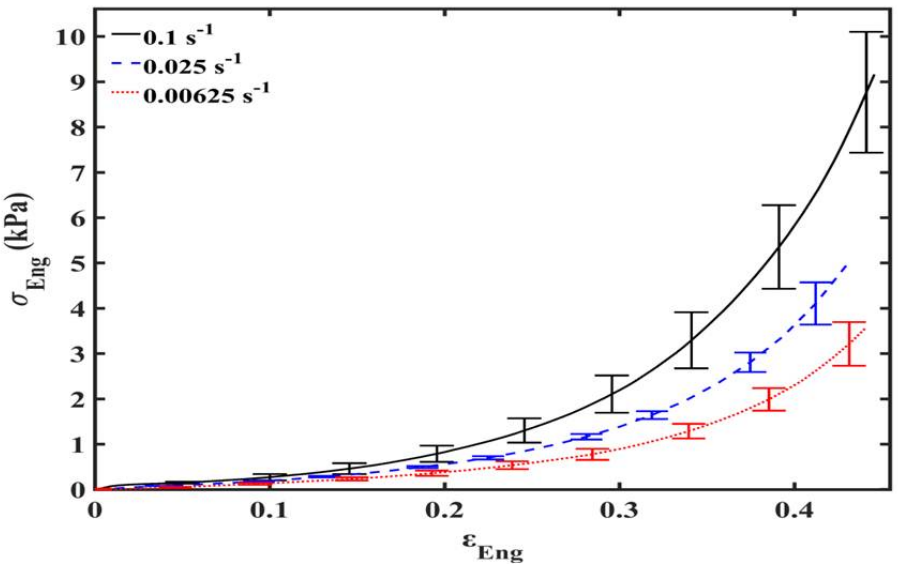

Figure 5.5 Comparison of stress-strain properties of porcine brain tissue compressed at strain rates of 0.1 s^{-1}, 0.025 s^{-1}, and 0.00625 s^{-1}.

(a) Adult porcine brain tissue to strain level of 40% adapted from Begonia et al.[1]
(b) Fetal porcine brain tissue to strain level of 45%.

This finding of higher stress, indicating a higher stiffness, in the fetal porcine brain after mechanical testing compared to that found in the adult brain, differs from what is found in literature. Weickenmeier et al. found using nanoindentation testing that immature, incompletely myelinated, brains were softer than mature brains.[16] Bovine

brains were used in the study, which are also further developed with greater myelination than a human brain at birth.[15] The nanoindentation method creates compression at a single, nanometer sized point of contact on the sample giving a nanoscale reading of the stress from the sample. The mechanics at smaller length scales are expected to have more stiff responses than at the macroscale.[17] The data collected in this study and by Begonia et al. was compressed across the entire cross-section of the sample giving a macroscale reading of the stress from the sample. Research done by Prange and Margulies was also conducted at the macroscale level on infant and adult porcine brain tissue. The shear and compression testing of samples containing both white and gray matter were compared and the infant samples in shear and compression were found to be stiffer than the adult samples.[10] Prange and Marguies findings support the comparison of the results of infant compression in this study and adult compression data by Begonia et al. The opposing findings in the comparison of mechanical data of infant and adult brain indicate why further study and understanding of the development of the brain are needed.

5.4 Clinical Implications

It is known that the underlying microstructure of an object greatly influences its mechanical properties.[9] This can be seen by the difference in the mechanical properties found in the testing of the white and grey matter of the brain.[16] The white matter consists of the long myelinated axons of the neuron within a network of neuroglial cells. The grey matter consists primarily of the cell bodies of the neuron, glial cells, and a network of dendritic connections.[7] This can also be seen in the difference of the mechanical properties found between adult and infant brain tissue. The compression of the fluid-filled cells in an aqueous environment causes more stress to compact the cells and force

the fluid out of the tissue than the amount necessary to separate the cells and force out the fluid in the tissue in tension.

The underlying microstructure of an object is also known to influence its functional properties. The body does everything it can to stay in a balance of temperature, pH, and cellular configuration for homeostasis. The brain has its own homeostatic configuration of neuronal and glial cells within the tissue important to proper functioning. A disruption of homeostasis in the CNS through deformation, such as from compressive or tensile loading, can produce a more compact array of cells as found in this study. The disruption of the homeostatic morphology of the brain can produce biological complications through processes such as traumatic axonal injury (TAI). TAI is the predominant mechanism for failure in white matter as a degenerative process started by a change in the neurons. Axon detachment can be attributed to the misalignment of the cytoskeleton, denser compaction of neurofilaments, and deterioration of microtubules causing TAI.[8] The disruption of neuronal cells in the CNS can also have an effect on the glial cells of the brain and vis versa. Oligodendrocytes, astrocytes, and microglia are the predominant glial cells in the CNS and are responsible for the regulation of proper neuronal function. Microglia detect changes in the CNS and are activated by neuronal damage. The signaling of damaged neurons produces functional changes in the microglial cells illustrating the significance of neuronal-microglial signaling to CNS tissue failure.[13] The research conducted in this study provides microstructural information on the area fraction and nearest neighbor distance after tissue loading. The findings of this study in Figure 4.8 indicate cell deformation, which increases with increased strain level and can point to cell function disruption in a physiologically capable test subject.

The compressive loading of the brain tissue caused the sample to decrease in height and increase in diameter while the tensile loading caused an increase in the sample height and decrease in the sample diameter. The microstructural changes that can occur after this compressive and tensile loading are important to know in order to understand how brain function can change after damage. The microstructure, coupled with *in vivo* testing to look into brain function changes after load and to understand the physiological implications of loading on the brain, can help to give a full picture of TBI in infants. The understanding can be implemented in the creation of more accurate and precise FE models of the infant brain. Currently FE models are not being created with a cellular component in full head models. The mechanical and microstructural data produced in this study can be used to help develop the morphology of such a model and be compared to other models for accuracy. The FE models can then be utilized for the development of better protective measures and equipment for infants.

5.5 References

1. Begonia, M. T., R. Prabhu, J. Liao, M. F. Horstemeyer, and L. N. Williams. The Influence of Strain Rate Dependency on the Structure–Property Relations of Porcine Brain. *Ann. Biomed. Eng.* 38:3043–3057, 2010.

2. Cernak, I. Animal models of head trauma. *NeuroRX* 2:410–422, 2005.

3. Coats, B., G. Binenbaum, C. Smith, R. L. Peiffer, C. W. Christian, A.-C. Duhaime, and S. S. Margulies. Cyclic Head Rotations Produce Modest Brain Injury in Infant Piglets. *J. Neurotrauma* 34:235–247, 2017.

4. Coats, B., S. A. Eucker, S. Sullivan, and S. S. Margulies. Finite element model predictions of intracranial hemorrhage from non-impact, rapid head rotations in the piglet. *Int. J. Dev. Neurosci.* 30:191–200, 2012.

5. Dickerson, J. W., and J. Dobbing. Prenatal and postnatal growth and development of the central nervous system of the pig. *Proc. R. Soc. London. Ser. B, Biol. Sci.* 166:384–95, 1967.

6. Dobbing, J. The later growth of the brain and its vulnerability. *Pediatrics* 53:2–6, 1974.

7. Goriely, A., S. Budday, and E. Kuhl. Chapter Two – Neuromechanics: From Neurons to Brain. *Adv. Appl. Mech.* 48:79–139, 2015.

8. Kelley, B. J., O. Farkas, J. Lifshitz, and J. T. Povlishock. Traumatic axonal injury in the perisomatic domain triggers ultrarapid secondary axotomy and Wallerian degeneration. *Exp. Neurol.* 198:350–360, 2006.

9. Meyers, M. A., P.-Y. Chen, A. Yu-Min Lin, and Seki Yasuaki. Biological materials: Structure and mechanical properties. *Prog. Mater. Sci.* 53:1–206, 2008.

10. Prange, M. T., and S. S. Margulies. Regional, directional, and age-dependent properties of the brain undergoing large deformation. *J. Biomech. Eng.* 124:244–52, 2002.

11. Raghupathi, R., M. F. Mehr, M. A. Helfaer, and S. S. Margulies. Traumatic Axonal Injury is Exacerbated following Repetitive Closed Head Injury in the Neonatal Pig. *J. Neurotrauma* 21:307–316, 2004.

12. Sillesen, M., L. S. Rasmussen, G. Jin, C. H. Jepsen, A. Imam, J. O. Hwabejire, I. Halaweish, M. DeMoya, G. Velmahos, P. I. Johansson, and H. B. Alam. Assessment of coagulopathy, endothelial injury, and inflammation after traumatic brain injury and hemorrhage in a porcine model. *J. Trauma Acute Care Surg.* 76:12–20, 2014.

13. Streit, W. J. Microglial Response to Brain Injury: A Brief Synopsis. *Toxicol. Pathol.* 28:28–30, 2000.

14. Thibault, K. L., and S. S. Margulies. Age-dependent material properties of the porcine cerebrum: effect on pediatric inertial head injury criteria. *J. Biomech.* 31:1119–1126, 1998.

15. Urban, K., M. Hewicker-Trautwein, and G. Trautwein. Development of Myelination in the Bovine Fetal Brain: an Immunohistochemical Study. *Anat. Histol. Embryol. J. Vet. Med. Ser. C* 26:187–192, 1997.

16. Weickenmeier, J., R. de Rooij, S. Budday, T. C. Ovaert, and E. Kuhl. The mechanical importance of myelination in the central nervous system. *J. Mech. Behav. Biomed. Mater.* 0–1, 2017.doi:10.1016/j.jmbbm.2017.04.017

17. Zhu, F., P. Skelton, C. C. Chou, H. Mao, K. H. Yang, and A. I. King. Biomechanical responses of a pig head under blast loading: a computational simulation. *Int. j. numer. method. biomed. eng.* 29:392–407, 2013.

CHAPTER VI

CONCLUSION

This study was conducted to find the structure-property relationship of fetal porcine brain for finite element modeling of TBI in infants and the characterization of the microstructural deformation after loading. Compression testing of fetal porcine brain resulted in a higher stress level than tensile testing (Figure 4.1, 4.2). This is most likely due to the stress created during compression when the glial cells and neuronal cells are being forced together in the aqueous environment creating an elevated stress while the underdeveloped neurons and the glial cells were more easily separated in tension. After both compression and tension testing was completed, the mean area fraction and mean nearest neighbor distance was found for microstructural analysis. The results of compression in the longitudinal and transverse cross-sections were both found to have shown a statistical change in the microstructure of the tested samples (Figure 4.4, 4.5). The longitudinal cross-section was found to be most influenced by the strain level while the change in microstructure of the transverse cross-section was most influenced by the strain rate. Tension testing resulted in statistically relevant change in the mean area fraction and mean nearest neighbor distance most notably in the longitudinal cross-section (Figure 4.6, 4.7). After tensile testing, both the longitudinal and transverse cross-section result was that neither the strain rate or strain level was a larger influence in the changes in the microstructure after load was applied. The statistically relevant changes in

the microstructure found after testing (Figure 4.8) and the increases in deformation (Figure 4.9) could indicate that a large enough change in the cell morphology has occurred to affect function.[2,3]

When the stress levels found in this study were compared to adult quasi-static testing of porcine brain tissue in compression, the stresses found by Begonia et al. were lower than those of the infant stress-strain data (Figure 5.5).[1] The difference in the mechanical data between the adult and infant porcine brain indicates the need to have specific mechanical data for all ages to understand the change in mechanics created over the course of brain development. The data provided in this study aids in the understanding of TBI by adding knowledge of the structure-property relationship of the infant brain under load. The mechanical and histological data can be used to create better testing models to understand infant TBI.

6.1 Limitations and Future Works

There are some limitations to this study that could be addressed in future work for validation of this study and to further the understanding of infant TBI. A limitation of this study is that the samples being dissected from the fetal piglets before testing means the physiological properties of live tissue cannot be analyzed to see how they would affect the microstructure under load. The microstructure of the fresh tissue can be analyzed but without the cells in the tissue being within a live specimen, the effects of cell death through the tissue cannot be fully analyzed.

Another limitation of this study is that the tension testing was not conducted in a PBS bath. The tension samples were kept hydrated before testing, but were conducted with the sample surrounded by air. The compression testing was done in a PBS bath to

create a physiologic environment for the sample. The aqueous environment could be an influence as to why the compression tests reached a much higher stress level than the tension testing. Future research could be conducted with the tensile testing conducted under physiologic conditions, utilizing a PBS bath, to compare to the compression tests.

The samples in this study were mechanically loaded during testing in both compression and tension, but not unloaded. In future testing, the results of loading and unloading of the samples should be found to allow for the calculation of energy dissipation. This will then provide knowledge of the energy loss under varying stress states and correlation with the structure-property relationship of the tissue.

Additionally in future testing the platen and stainless steel container used for compression of the samples should have a frictionless surface. A frictionless surface would prevent possible barreling of the samples and eliminate it as an influence in the studies findings. The findings of such a study would also help to understand the results of this study.

Finally, in a future study image analysis of more than one area on the histological slides would help to give a more global understanding of the morphological changes occurring in the tissue after loading. The results from the histological images at the center of the samples can then be compared to the findings of this study to determine the possible edge effect in the results. Further image analysis would assist in building on the structure-property findings of this study and increase the understanding of infant TBI.

6.2 References

1. Begonia, M. T., R. Prabhu, J. Liao, M. F. Horstemeyer, and L. N. Williams. The Influence of Strain Rate Dependency on the Structure–Property Relations of Porcine Brain. *Ann. Biomed. Eng.* 38:3043–3057, 2010.

2. Kelley, B. J., O. Farkas, J. Lifshitz, and J. T. Povlishock. Traumatic axonal injury in the perisomatic domain triggers ultrarapid secondary axotomy and Wallerian degeneration. *Exp. Neurol.* 198:350–360, 2006.

3. Streit, W. J. Microglial Response to Brain Injury: A Brief Synopsis. *Toxicol. Pathol.* 28:28–30, 2000.